NASA CONTRACTOR REPORT

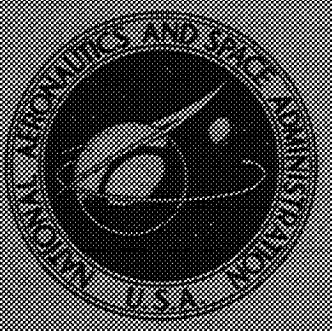

NASA CR-2218

NASA CR-2218

Corrected Copy

ANALYSIS AND DESIGN OF ADVANCED COMPOSITE BONDED JOINTS

by L. J. Hart-Smith

Prepared by
DOUGLAS AIRCRAFT COMPANY
MCDONNELL DOUGLAS CORPORATION
Long Beach, Calif. 90846
for Langley Research Center

NATIONAL AERONAUTICS AND SPACE ADMINISTRATION • WASHINGTON, D. C. • AUGUST 1974

1. Report No. NASA CR-2218	2. Government Accession No.	3. Recipient's Catalog No.
4. Title and Subtitle ANALYSIS AND DESIGN OF ADVANCED COMPOSITE BONDED JOINTS		5. Report Date August 1974 6. Performing Organization Code
7. Author(s) L. J. Hart-Smith		8. Performing Organization Report No.
9. Performing Organization Name and Address Douglas Aircraft Company, McDonnell Douglas Corporation, 3855 Lakewood Blvd, Long Beach, California 90846.		10. Work Unit No. 11. Contract or Grant No. NAS1-11234
12. Sponsoring Agency Name and Address National Aeronautics and Space Administration, Washington, DC 20546.		13. Type of Report and Period Covered Contractor Report - Final 14. Sponsoring Agency Code

15. Supplementary Notes

Related information is to be found in the four technical reports NASA CR-112235, -6, -7, and -8 which were prepared under the same NASA Langley contract governing this summary report.

16. Abstract

Advances in the analysis of adhesive-bonded joints are presented in this report, with particular emphasis on advanced composite structures. The joints analyzed are of double-lap, single-lap, scarf, stepped-lap and tapered-lap configurations. Tensile, compressive, and in-plane shear loads are covered. In addition to the usual geometric variables, the theory accounts for the strength increases attributable to adhesive plasticity (in terms of the elastic-plastic adhesive model) and the joint strength reductions imposed by imbalances between the adherends. The solutions are largely closed-form analytical results, employing iterative solutions on a digital computer for the more complicated joint configurations. In assessing the joint efficiency, three potential failure modes are considered. These are adherend failure outside the joint, adhesive failure in shear, and adherend interlaminar tension failure (or adhesive failure in peel). Each mode is governed by a distinct mathematical analysis and each prevails throughout different ranges of geometric sizes and proportions. All joints with uniformly thick adherends are shown to be limited in utility beyond determinable adherend thicknesses. The adhesive film strain energy in shear per unit bond area is demonstrated to be the dominant measure of the influence of the adhesive on the joint strength. Agreement with available experimental evidence is indicated. As well as the basic joint configurations, the theory has been applied to a variety of non-classical joint configurations which occur frequently in practical aerospace constructions. These include bonded doublers and joint details associated with selective reinforcement of metal structures by advanced composites.

17. Key Words (Suggested by Author(s))

Adhesive-Bonded Joints
Double-Lap Joints
Single-Lap Joints
Scarf Joints,
Stepped-Lap Joints
Tapered-Lap Joints
Adhesive Plasticity
Adherend Thermal Mismatch
Adherend Stiffness Imbalance
Adhesive Shear Failures
Adhesive Peel Failures
Digital Computer Programs

18. Distribution Statement

Unclassified - Unlimited

Cat. 32

19. Security Classif. (of this report)	20. Security Classif. (of this page)	21. No. of Pages	22. Price*
Unclassified	Unclassified	60	$3.75

* For sale by the National Technical Information Service, Springfield, Virginia 22151

FOREWORD

This report was prepared by the Douglas Aircraft Company, McDonnell Douglas Corporation, Long Beach, California under the terms of Contract NAS1-11234. One summary report (NASA CR 2218) and four technical reports (NASA CR 112235, -6, -7, and -8) cover the work, which was performed between November 1971 and January 1973. The program was sponsored by the National Aeronautics and Space Administration's Langley Research Center, Hampton, Virginia.

CONTENTS

ANALYSIS AND DESIGN OF ADVANCED COMPOSITE BONDED JOINTS

By L. J. Hart-Smith

Douglas Aircraft Company, McDonnell Douglas Corporation

SUMMARY

Advances in the design of adhesive bonded joints are presented in this report, with particular reference to advanced composite structures. The solutions are largely closed-form analytical results, employing iterative solutions on a digital computer for the more complicated joint configurations. The joints analyzed are of double-lap, single-lap, scarf and stepped-lap configurations. Tensile, compressive, and in-plane shear load conditions are covered. In addition to the usual geometric variables, the following joint parameters are accounted for: adhesive plasticity (using an elastic-plastic shear stress model), adherend stiffness imbalance and adherend thermal mismatch. Of these, the adhesive plasticity increases the joint failure strength dramatically above the predictions of purely elastic analyses because the maximum lap-joint strengths are shown to be defined by the adhesive strain energy in shear. Any dissimilarity between adherends effects a joint strength reduction.

In assessing the joint efficiency, three potential failure modes are considered. First, for a well-designed joint, the laminate (adherend) will fail outside the joint. This failure mode is particularly prevalent for single-lap joints but they should not be considered well-designed because of the eccentricity in the load path. Second, the ultimate shear strain of the adhesive may be exceeded, resulting in bond failure. This is the usual test case. Third, the peel stresses induced at the end(s) of the joint may exceed the interlaminar tension strength of the laminate, causing a splitting failure of the adherend. (In the case of metal adherends, the corresponding failure is by peeling the adherends apart.) This third mode applies particularly to thick section lap joints and occurs for both single-lap and double-lap joints, at loads far below the potential bond shear strength. A simple modification is suggested which virtually eliminates the peel-stress problem.

The analyses on which this report is based are documented in four separate technical reports, so mathematical derivations are excluded from this report. The digital computer programs used in preparing the solutions are to be found in the same references which are in the text. Practical considerations of design, analysis, and fabrication are also discussed.

INTRODUCTION

In realizing the full potential of the advanced composites (boron and graphite) in lightweight aircraft structures, it is particularly important to ensure that the joints, either bonded or bolted, do not impose a reduced efficiency on the structure. This problem is far more severe than with conventional metals, such as aluminum, titanium, and steel, because the high-specific-strength filaments are relatively brittle. They have very little capacity to redistribute loads and practically none of the forgiveness of a yielding metal to mask a multitude of design approximations. This is the reason why great efforts are devoted to understanding joints in composite materials and to providing reliable design techniques. While much has been accomplished, much remains to be done, particularly for the thicker sections and for multiple fastener patterns.

The purpose of this report is to provide analytical techniques for bonded joints, which are both simple enough for design purposes and yet include sufficient parameters to provide good correlation between test and theory. The concept employed is that of elastic-plastic adhesive analyses developed at the Douglas Aircraft Company and greatly expanded in application through this NASA Langley Research Center contract. Special emphasis is placed upon non-dimensionalized solutions in terms of the governing parameters to illustrate the overall joint behavioral phenomena in terms of three characteristic failure modes. The failure modes are isolated into laminate-induced failures, adhesive shear failures and adhesive peel induced failures because it is good design practice for reliability to aim for a potential adhesive strength significantly in excess of that of the adherends being joined.

Stresses and strains induced in a bond under load arise from the differential movement of the adherends bonded together. Were the adhesive shear stress an inherent constant property, like the surface tension of a soap-bubble membrane, design would be straightforward. It is not, so the three basic sources of non-uniform adhesive shear strain must be accounted for. These are discussed below with reference to double-lap joints, but exactly the same phenomena occur in single-lap, stepped-lap, and scarf joints (albeit governed by differential equations of different type).

First, there is the strain concentration due to adherend extensibility, depicted in Figure 1 for identical adherends. It is apparent that stiffer adherends promote more efficient bonds. However, stiffer adherends are usually associated with greater adherend strengths (and hence bond loads) and while the load essentially increases proportionally with the adherend thickness, the bond capacity increases less rapidly, being proportional to the square root of the adherend thickness. It is inevitable that, all other variables remaining constant, efficient double-lap joints are restricted with respect to adherend thickness. This is the reason why scarf joints or stepped-lap joints are employed for thicker sections.

Second, and this cannot be avoided for scarf joints either, there is the influence of adherend stiffness imbalance, shown in Figure 2. The adhesive shear strains are intensified at the end from which the softer (less stiff) adherend extends. This same end is critical whether the shear load be tensile or compressive. In comparison with a stiffness-balanced joint, this imbalance reduces the joint strength by unloading the less critical end. In a balanced joint there is an equally effective area of adhesive at each end of the joint.

Third, there is the case of adherend thermal mismatch, which is acute for the aluminum-to-graphite epoxy combination and still significant for titanium-to-boron epoxy. The problem arises because high-strength adhesives are customarily cured at temperatures far above their operating temperature. The mechanics of this imbalance are portrayed in Figure 3, with the metal (higher coefficient of thermal expansion) sandwiched in the middle. The metal tends to shrink as temperature is decreased from the cure value and is partially resisted by the composite (lower thermal coefficient of expansion) outer adherends,

thereby setting up residual bond stresses. The important characteristic of the so-called thermal stress imbalance is that the critical end of the joint changes with the direction of application of the load. With all other variables constant, this problem becomes progressively more severe with increasingly thick adherends, to the extent that some joints are observed to break apart while cooling down in the autoclave after curing of the adhesive, without the application of any external load.

It is appropriate to explain here also how for uniform lap joints the load is actually transferred through two end zones (or only one in the case of severely unbalanced joints) with a lightly-loaded elastic trough in-between, as shown in Figure 4. The extent of these end zones is defined largely by the adhesive plasticity. Increasing the total overlap of uniform thickness adherends, for all but very short overlaps, merely moves the effective end zones further apart without changing the load transferred or the maximum adhesive stresses and strains developed. Scarf and stepped-lap joints differ somewhat from uniform lap joints inasmuch as that, while they also contain limited plastic zones of adhesive, the load transferred by the elastic zone increases indefinitely with longer overlaps. The dominant characteristic of scarf joints is that, regardless of all other factors, the ratio of the average bond shear stress to the peak bond shear stress equals the lower ratio of the adherend extensional stiffnesses. This is why such joints retain their effectiveness for thicker sections than can be joined efficiently by uniform lap joints.

The remaining dominant characteristic of adhesive-bonded joints is the peel stresses developed in association with the shear stresses. Like the shear stresses, these peak at the ends of the joint. While this phenomenon has long been known for single-lap joints, it is only recently that its impact on inducing laminate failures in thick double-lap joints was recognized. The low interlaminar tension strength of composite laminates limits the thickness of the adherends which can be bonded together efficiently by lap joints. The inner laminate splits apart locally due to peel stresses, thereby destroying the shear transfer capacity between the inner and outer plies. This overloads the outer filaments, which break in tension, and the failure progresses as portrayed in Figure 5. The effect of this failure mode is to restrict the thickness of composites which can be bonded efficiently using standard double-lap

and single-lap joints. Techniques to alleviate this problem are discussed in the text and revolve around tapering the end of the outer adherend to minimize the peel stresses developed. A significant improvement in the shear strength can be associated with this simple modification.

The understanding of these basic phenomena permits the development of a rational basis for the design of bonded joints.

The basis of the present analyses of adhesive-bonded joints is the idealized elastic-plastic stress-strain characteristic of the adhesive film in shear, as shown in Figure 6. There are several reasons behind the choice, some of which are discussed in greater detail in Reference 1. This reference also discusses some history of nonlinear adhesive-representations and explains the need for accounting for such nonlinearities to reconcile theory and experiment. The available ductile structural adhesives are effectively limited to below 250° F operating environments and the loss in strength at low temperature is the price that has been paid for retaining high-temperature strength, as shown in Figure 7.

Having recognized the need for representing the adhesive non-linear behavior and accepted the use of the elastic-plastic characterization for the mathematical model, there remains the need to define the mathematical model in terms of the actual characteristic. The process adopted here and the justifications for each step follow and are illustrated in Figure 6. The ultimate shear strains are matched because they provide the failure criterion in the analysis. The plastic shear stress is set at the maximum value developed on either a torsion-ring or thick-adherend shear specimen. This value governs the behavior of joints having relatively short overlaps. The elastic strain is then set at that value for which the strain energy of the idealized characteristic matches that for the actual curve. The strain energy alone is the necessary and sufficient definition of the influence of the adhesive on the maximum potential bond shear strength (see References 2 and 3). Any adhesive idealization defined by two straight lines having the same strain energy and failure stress and strain predicts precisely the same maximum joint strength that can be developed between given uniform adherends.

The formulation above of the idealized adhesive characteristic corresponding to the actual curve pertains to analysis. Slight modifications are required for design. The peak allowable shear stress should be multiplied by a factor of 0.8 (based on visual observation of many specimens) to account for the incomplete wetting of the adherend by the adhesive. The need for this factor arises from both the difference between laboratory and production fabrication and the greater production bond areas on which surface waviness causes proportionally more voids. There is relatively little experimental scatter of the peak bond shear stress. More scatter is recorded for the failure strain. An average value should be adopted, just as for the peak shear stress. In converting the experimental failure strain to an effective allowable, two approaches are available. In the first, a certain fraction of the ultimate strain could be used. The second, which is recommended here, is that for the allowable ultimate adhesive shear strain the potential bond strength should exceed the adherend strength by at least 50 percent. Therefore, when the more critical adherend has attained ultimate load, the adhesive will not have developed its ultimate shear strain. The need for such a reserve factor arises principally from the environmental degradation suffered by bonded joints during service. Building in excess strength initially promotes longer effective lives for bonded structures without significant weight penalties. A reserve of 25 percent is recommended for failures governed by interlaminar tension in laminates because they do not deteriorate as fast as the adhesive-to-adherend interfaces. It is obviously not always possible to achieve these margins without redesign of initial joint concept geometries, particularly for thicker laminates. However, the additional effort is justified by the increase in overall structural efficiency achieved by having failures confined to outside the joints.

The closed-form analytical studies reported in References 2 to 5 show that the adhesive shear strain occurs as a product with the adhesive film thickness. It is differential adherend displacement, across the bond-line, which determines the joint strength rather than the adhesive film thickness and maximum shear strain separately. This makes it unnecessary to measure precisely the bond-line thicknesses. This does not suggest that the thickness is unimportant; it obviously influences the properties of the adhesive layer. Generally, adhesive layers have proved optimum at about 0.1 to 0.15 mm (0.004 to 0.006 inches) thick.

Starved glue lines (less than 0.05 mm thick) represent obvious weaknesses, while excessively thick layers are usually found to be inferior because of excessive voids.

Typical room-temperature properties of adhesives are summarized in Table 1. These values vary somewhat for different operating temperatures, as shown in Figure 8, but little data has yet been published for other than room temperatures. Only recently has the need for complete stress-strain curves as a basis for design been recognized. However, one observation is warranted with regard to the use of adhesives on commercial transport aircraft. As the temperature is reduced towards the lower limit of 218 K (-67°F), the adhesive becomes both less ductile and stronger while, at the upper limit of 344-355 K (160-180°F), the adhesive is weaker but more ductile. The effective changes in strain energy appear to be small throughout this operating range, so joint strength variation with temperature is not expected to be a major problem.

The discussion above on adhesive characterization for design and analysis has been confined to ultimate static strength. The equally important problem of fatigue performance of bonded joints is associated with partial load levels. Fatigue, rather than static strength, governs much of the design of mechanically fastened metal aircraft structures. A related factor is the decrease in residual structural strength with age and environmental exposure. Adhesive bonds are known to deteriorate in service, just as mechanically fastened metal structures do. Therefore, the design process accounts for this variation in structural behavior during service life of the aircraft. Consequently, it appears likely that the entire static shear strain capacities of ductile adhesives cannot be fully utilized for commercial transport aircraft. This has led to a supposition that brittle adhesives may be more suitable for aircraft use than are ductile adhesives. However, the fatigue performance of ductile and brittle adhesives should not be judged on the basis of the ratio of static and fatigue run-out strengths; the appropriate measure for each adhesive is cycles to failure under the same loads applied to joints having identical adherends. On this basis, experimental evidence (Reference 6) demonstrates the superiority of ductile adhesives over the brittle adhesives in fatigue. Figure 9 shows a comparison of representative ductile and brittle adhesives in terms of their real shear properties, obtained from torsion ring tests, rather

than the ambiguous strength measurements obtained on standard one-half inch single-lap test coupons. Since maximum bond strength is proportional to the square root of the area under the curves, it is seen that ductile adhesives possess several times the load transmission capability of brittle adhesives. Thus a fatigue designed ductile bond would possess a much higher static margin of safety than would a fatigue designed brittle bond. This added margin has proven to be invaluable for the redistribution of load around local stress concentrations.

Another aspect of adhesive characterization is the stress-strain behavior in peel, which is influenced greatly by the in-plane restraint of the adjacent stiff adherends. The need for such information has not been recognized for long enough for a significant bank of pertinent data to be established. Just as the shear properties of adhesives films vary somewhat with thickness and differ markedly from the bulk properties, so do the peel properties. The analyses for peel stresses are consequently formulated in terms of an effective linear elastic transverse modulus of the adhesive layer, and it is recognized that more experimental work remains to be done in this field.

The reason for restricting the peel stresses to their elastic limits is that, for composite adherends, the peel-stress induced failure occurs within the laminate as soon as the peel stress exceeds the interlaminar tension strength of the laminate. Since this latter strength is far less than the peel strength of typical structural adhesives, there is no need to complicate the analysis unnecessarily. This comment does not hold for metal adherends, of course, with which adhesive peel failures are not uncommon. In any event, if the elastic peel stress problem with a given design is sufficiently severe to warrant consideration of an elaborate analysis, it is usually better to incorporate peel stress relief in the design because peel stresses are only a problem if the joint efficiency is low. Techniques for modifying the basic uniform lap joint to achieve such relief are discussed below. The peel stress analyses serve also to identify the thicknesses of adherends beyond which more efficient scarf or stepped-lap joints are needed. The elastic analysis is somewhat conservative for metals but accurate for composites. While the peel stress analyses may lack the precision associated with the shear stress analyses they show that, for uniform lap joints, the peel stresses are more crucial than shear

stresses in determining the adherend thickness at which it is necessary to employ the more efficient scarf or stepped-lap joints.

SYMBOLS

a, b extents of plastic stress state in adhesive at ends of bonded joint (m)

c half-length of single-lap joint overlap (m)

CPEEL non-dimensionalized peel stress coefficient

$$\text{CPEEL} = \left(\frac{E_c' t}{E\eta}\right) 3(1-\nu^2)$$

CTHERM non-dimensionalized adherend thermal mismatch coefficient

$$\text{CTHERM}(1) = \frac{(\alpha_2 - \alpha_1)\Delta T\lambda}{\tau_p\left[\frac{1}{E_1 t_1} + \frac{1}{E_2 t_2}\right]}, \quad \text{CTHERM}(2) = \frac{(\alpha_1 - \alpha_2)\Delta T\lambda}{\tau_p\left[\frac{1}{E_2 t_2} + \frac{1}{E_1 t_1}\right]}$$

D flexural rigidity of adherends (Nm^3)

d length of elastic zone in adhesive bond (m)

E Young's modulus (longitudinal) for adherend (N/m^2)

e eccentricity (m)

E_c, E_c' adhesive peel (transverse tension) modulus (N/m^2)

ETR adherend extensional stiffness ratio

$$\text{ETR}(1) = E_1 t_1 / E_2 t_2 , \quad \text{ETR}(2) = E_2 t_2 / E_1 t_1$$

F_u, F_y ultimate and yield adherend allowable strengths outside joint (N/m^2)

G adhesive elastic shear modulus (N/m^2)

k eccentricity factor for single-lap joints

$$k = 2M_o/Pt$$

k_b non-dimensionalized bending stiffness parameter for filamentary composite adherends

$$k_b = D/[Et^3/12(1-\nu^2)]$$

ℓ overlap (length of bond) (m)

M bending moment per unit width of adherend (Nm/m)

M_o bending moment in adherend at end of overlap (Nm/m)

P applied load on joint per unit width (N/m)

t thickness of adherend (m)

T temperature (K)

ΔT temperature change ($T_{operating} - T_{stress\text{-}free}$) (K)

α coefficient of thermal expansion (/K)

γ adhesive shear strain

γ_e elastic adhesive shear strain

γ_{max} maximum total adhesive shear strain

γ_p plastic adhesive shear strain

η thickness of adhesive layer (m)

η joint efficiency

$$\eta = P/F_u t \quad \text{or} \quad P/F_y t$$

λ exponent of elastic shear stress distribution in adhesive (m^{-1})

$$\lambda^2 = \frac{G}{\eta}\left[\frac{1}{E_1 t_1} + \frac{1}{E_2 t_2}\right]$$

This serves as a non-dimensionalizing factor for the overlap ℓ.

ν Poisson's ratio for adherends

σ_c, σ_p peel stresses in adhesive (N/m^2)

σ_y yield stress in adherend (N/m^2)

τ adhesive shear stress (N/m^2)

τ_{av} average adhesive shear stress (N/m^2)

τ_p plastic adhesive shear stress (N/m^2)

Subscripts:

a, c adhesive (cement)

i, o inner and outer adherends of double-lap bonded joint

$1, 2$ / $1, 4$ adherends at opposite ends of single-lap joint

n property normal to plane of adherends

DOUBLE-LAP JOINTS

The classical elastic solution for double-lap bonded joints is that of Volkerson (Reference 7)*. This derivation and the similar one by de Bruyne (Reference 8)* are purely-elastic analyses and include adherend stiffness imbalance but not thermal mismatch. The analysis herein used these techniques as a foundation and also included adhesive plasticity and adherend thermal mismatch.

The complete mathematical details of the analysis is published in Reference 2, so only an outline of the technique is presented here. The solution is performed in terms of the adhesive shear strain rather than stress because of the non-uniqueness of the shear strain in the plastic zone. Figure 10 depicts the geometry, nomenclature, and factors included in the analysis of a symmetric double-lap joint. The solution proceeds from force-equilibrium for the differential elements of adherends, and stress-strain relations for the adherends and for the adhesive, through compatibility equations ensuring continuity of the bond, to one governing differential equation for the elastic adhesive zone and another for the plastic zone(s). These are solved and the boundary conditions satisfied at the elastic-to-plastic transition(s) and at the joint extremities. The computer program developed for the solution is listed in Reference 2. The complete non-dimensionalized solution for balanced double-lap joints is depicted in Figure 11, in which the ordinate defines the joint strength and the abscissa the joint overlap. Large increases in joint strengths are predicted when adhesive plasticity is included in the analysis. The joint load is proportional to the overlap for short (fully-plastic) overlaps, while no further strength is to be gained by increasing the overlap beyond that indicated as the optimum design line. The "plateau" strengths are

---

* Strictly speaking, the presentations are illustrated with single-lap joints, but the analyses lack the factors accounting for the eccentric load path. Consequently, they pertain to one half of a double-lap joint and are valid for such, subject to the limitations defined above.

defined by the simple relation

$$\frac{\tau_{av}}{\tau_p}\left(\frac{\lambda \ell}{2}\right) = \sqrt{1 + 2\left(\frac{\gamma_p}{\gamma_e}\right)} \qquad (1)$$

for balanced double-lap joints. In this non-dimensionalized relation, τ_{av}/τ_p is the ratio of average adhesive shear stress to maximum (plastic) shear stress, $\lambda\ell$ is a non-dimensionalized joint overlap (so that $\tau_{av}\ell$ is proportional to joint strength) and γ_p/γ_e is the ratio of plastic to elastic adhesive shear strain. Figure 12 shows the influence of lap length on the bond shear stress distribution. The analysis predicts that for balanced adherends each plastic zone has a characteristic length $(\ell-d)/2$ given in non-dimensionalized form as

$$\frac{\lambda(\ell - d)}{2} = \sqrt{2\left(\frac{\gamma_p}{\gamma_e}\right)} = \text{constant} \quad , \qquad (2)$$

which is independent of the total overlap. The greater the adhesive plasticity, the greater is the extent of the plastic end zones. The maximum adhesive shear stresses and strains are identical for each of the configurations A, B and C.

Returning to equation (1), in order to explain the significance of the adhesive strain energy in shear, re-arrangement leads to the explicit expression for the maximum shear load transferrable as

$$P = 2\tau_{av}\ell = \sqrt{4n\tau_p(\tfrac{1}{2}\gamma_e + \gamma_p)4E_o t_o} \quad . \qquad (3)$$

In this expression, the quantity $\tau_p(\frac{1}{2}\gamma_e + \gamma_p)$ represents the area under the stress strain curve per unit volume of adhesive, so the product with n converts it to the shear strain energy per unit area of bond. Note that no other adhesive properties influence the maximum potential bond shear strength of the joint The adherend influence, given by the extensional stiffness $E_o t_o$, shows how greater stiffness increases the potential bond shear strength, but not as fast as the greater thickness increases the strength of the adherends.

The equations above have been restricted to balanced joints in order to illustrate the effects of adhesive plasticity on the predicted joint strengths. When the effects of dissimilar adherends are included in the analysis, the predictions have the same form but the "plateau" strengths are reduced. Considering first the strength reduction due to stiffness imbalance alone, Figure 13 provides a correction factor to be applied to the "plateau" strength predictions for a balanced joint. In Figure 13 the outer adherends are the common reference between the balanced and unbalanced sets of adherends. Figure 14 shows how adherend thermal mismatch (dissimilar coefficients of thermal expansion α_o and α_i) reduces the maximum joint strength in the absence of any stiffness imbalance. Figure 15 explains how adherend thermal mismatch imposes proportionally greater strength reductions on brittle adhesives than on ductile ones. The reference temperature is strictly the stress-free temperature of the bond. Tests have shown that, for long hybrid composite strips, the stress-free temperature is the cure-initiation temperature of the adhesive which is usually slightly below the normal cure temperature. That is, for 394 K (250°F) curing adhesives, the stress-free temperature is about 380 K (225°F) even if the adhesive is heated to 450 K (350°F) during the cure (see Reference 9). Tests (Reference 9 and elsewhere) have demonstrated that, if the overlap is so long as to be beyond the capacity of the adhesive to relieve the thermal stress by creep, no significant thermal stress alleviation can be anticipated.

In the general case of unbalanced adherends in a double-lap joint, the theory predicts that the more critical end of the joint may not be identifiable by inspection and that the maximum possible bond shear strength for a given set of adherends is specified by the lesser of the following pair of equations.

$$P = 2\tau_{av}\ell = (\alpha_o - \alpha_i)\Delta T E_i t_i + \sqrt{2k\tau_p n(\gamma_e + \gamma_p)2E_i t_i[1 + (E_i t_i / 2E_o t_o)]} \quad (4)$$

$$P = 2\tau_{av}\ell = (\alpha_i - \alpha_o)\Delta T 2E_o t_o + \sqrt{2k\tau_p n(\gamma_e + \gamma_p)4E_o t_o[1 + (2E_o t_o / E_i t_i)]} \quad (5)$$

where

$$\Delta T = T_{operating} - T_{stress\text{-}free} \quad (6)$$

and

$$k = (\tfrac{1}{2}\gamma_e + \gamma_p) \,/\, (\gamma_e + \gamma_p) \tag{7}$$

is determined from the adhesive stress-strain characteristic. The product $n(\gamma_e + \gamma_p)$ is equal to the maximum bond-line shear displacement. The lower positive value of joint strength P is adopted and, if either estimate of P is negative, it means that the joint will break apart (without external load) because of excessive internal thermal stress. The necessary minimum overlap to realize the full shear strength of a bond is

$$\ell_{\text{practical design}} = \frac{P}{2\tau_p} + \frac{2}{\sqrt{\dfrac{\tau_p}{\eta\gamma_e}\left(\dfrac{1}{E_o t_o} + \dfrac{2}{E_i t_i}\right)}} \,. \tag{8}$$

Equations (4) and (5) are formulated for tensile lap-shear loading. Application of compressive shear loads instead may change the critical end of the joint, as explained above. In this case, the theory requires re-evaluation of equations (4) and (5) after changing the sign of the temperature differential ΔT. (Actually all other quantities in the analysis change sign, while this does not.) Thus, in the presence of adherend thermal mismatch, a double-lap adhesive-bonded joint may exhibit markedly different strengths for tensile and compressive shear loadings. For in-plane (edgewise) shear loading (see Figure 16), the same formulas apply, with changes to some of the parameters. The adherend extensional stiffnesses Et are replaced by their shear stiffnesses Gt and the thermal mismatch effects are just ignored because they develop adhesive shear strains perpendicular to those developed by the shear load. For severe thermal mismatch, however, thermally-induced adhesive shear strains developed at the sides of the joint are aligned with those caused by the in-plane shear load and the joint strength is restricted by critical local conditions at one or more corners of the bond area. This complex problem remains to be solved.

For certain combinations of dissimilar adherends both the stiffness and thermal imbalances will reinforce each other, often to the extent that only one

plastic zone will be developed in the adhesive. For other combinations the imbalances will nullify each other, resulting in a stronger joint (for one direction of loading) than for each imbalance alone. Unfortunately this is inevitably associated with a markedly reduced strength for loading in the opposite direction. Figure 17 illustrates some of these phenomena for unbalanced joints. Equations (4) through (8) apply for all of these situations and even encompass the purely-elastic case with no plastic zones at all.

Figure 18 presents a comparison of the theoretical predictions of this elastic-plastic theory with published test results (Reference 10) of small scale double-lap composite joints. The theoretical predictions are shown to lie within the experimental scatter.

A well-designed bonded joint, by definition, is one that exhibits failures outside the joint area. This makes it necessary to compare the potential bond strengths predicted by equation (4) or (5) with the adherend strength. Figure 19 illustrates the theoretical maximum bond strengths and minimum overlap requirements for aluminum double-lap joints bonded with a ductile adhesive cured at 394 K (250°F). Peel stress effects are not included. It is seen in Figure 19 that the bond to adherend strength ratio is much greater than unity for thin adherends and much less than unity for thicker adherends. The kink in Figure 19 is associated with a change in mode of failure from failure of the adherend outside the joint to failure of the adhesive in shear. This transition occurs at an inner adherend thickness of 6mm (0.25 inch) for the materials shown. The design overlap for thin joints which do not fail within the overlap region is given by the simple formula

$$\ell = \frac{\text{adherend strength}}{2 \times \text{peak bond shear stress}} + \frac{2}{\lambda} + \text{tolerance} \qquad (9)$$

Figure 19 includes only the effective plastic zones (the first term).

The limited shear transfer capability of bonded joints between adherends in excess of some thickness (dependent upon the materials and geometry) is well recognized. However, for still thicker adherends, the failure is initiated by peel forces rather than shear forces in the adhesive. A solution (Reference 2),

based on assumed elastic peel characteristics of the adhesive is shown in Figure 20 in non-dimensionalized form. The explicit solution for the peel stress as a function of the peak bond stress is

$$\frac{\sigma_p}{\tau_p} = t_o\left(\frac{E_c'}{4Dn}\right)^{\frac{1}{4}} = \left(\frac{3E_c'(1-\nu^2)t_o}{En}\right)^{\frac{1}{4}} \qquad (10)$$

In equation (10), the ratio σ_p/τ_p relates the peak peel stress to the peak shear stress (both at the end of the overlap), while E_c' is the effective transverse (peel) modulus of the constrained adhesive layer, t_o/n is the ratio of the outer adherend and adhesive layer thicknesses, and E is the Young's modulus for the outer adherend.

It is shown in Figure 20 that, beyond a certain thickness of adherend, the peel stresses developed in the bond exceed the peak shear stresses. Figure 20 shows also that, for sufficiently thin adherends, peel stresses are not a problem as long as the peel strength (and interlaminar tensile strength) is approximately equal to the shear strength. These predictions are in accord with the experimental evidence. It is apparent from Figure 20 that failures of double-lap joints of thick adherends cannot be explained by a shear stress distribution or by in-plane laminate stresses alone. Techniques to reduce the peak peel stress at the ends of the joint are illustrated in Figure 21. These are discussed further in the section on practical joints.

The concept of variable-stiffness (or mixed-modulus) adhesive bonded joints also has merit for peel-stress relief. A significant effort has been devoted to this concept (see Figure 22) to increase the shear strength of bonded joints. The aim has been to increase the total load transferred by using a stiff (high-modulus) adhesive in the middle of the joint where the adherend relative displacements are very small and a soft (low modulus) adhesive at the ends where such displacements are greater. On the basis of a purely-elastic assessment, such a scheme has considerable merit. The weakness in this assessment has been the neglect of adhesive plasticity, as shown in Figure 22. While the mixed-modulus adhesive concept has no practical merit in comparison with a ductile adhesive alone, it does offer advantages over a brittle adhesive alone. In high-temperature environments which preclude the efficient use of ductile

adhesives, a brittle adhesive (which retains its strength at high temperatures) may effectively transfer all the shear load while the weaker ductile adhesive protects the ends of the overlap, enabling the brittle adhesive to develop a higher average stress prior to failure.

As explained in the sections above, the efficiency of thick double-lap joints will inevitably be less than unity. That is, the joint will be weaker than the adherends. The pertinent phenomena are illustrated in Figure 23 for the high-strength graphite-epoxy and Figure 24 for aluminum. The material properties on which they are based are given in Table 2. These figures include a comparison of the relative efficiencies of ductile and brittle adhesives at room temperature. Diagrams such as these, prepared from the non-dimensionalized shear-stress and peel-stress analyses, identify the adherend thicknesses above which peel-stress relief is necessary as well as those for which a change to the more efficient scarf or step-lap joints is necessitated due to limited shear capacity. The charts present the "plateau" shear strengths and assume that adequate overlap is provided. These representative charts are presented for balanced joints, but the same technique can be applied for joints with dissimilar adherends also.

SINGLE-LAP JOINTS

Unlike the straightforward double-lap joint analyses, the solution of single-lap joint problems is complicated by the eccentricity in the load path. The first to account for this factor were Goland and Reissner (Reference 11) in 1944, in a purely-elastic analysis. The elastic-plastic analysis summarized herein is presented in detail in Reference 3 where differences between solutions are discussed. The co-ordinate system used in the elastic-plastic solution of Reference 3 is shown in Figure 25 along with characteristic bond stress distributions and identification of the factors included in the analysis. The solutions derived indicate that the eccentric load path imposes a severe reduction in joint efficiency.

The maximum stresses within and outside the unsupported single-lap joint are influenced greatly by the value of the bending moment M_o induced, just outside the overlap, by the eccentricity in the load path. The theory (Reference

3) predicts that this moment M_o is related to the applied load P by the equation

$$M_o = Pt \Big/ \left\{2[1 + (\xi c) + \tfrac{1}{6}(\xi c)^2]\right\} \qquad (11)$$

where $\xi^2 = P/D$ (D being the adherend bending stiffness), and c is half the overlap and t the thickness. The moment, along with its associated stress concentrations, is seen to be diminished by increasing the overlap. This feature is the dominant characteristic of the single-lap joint analysis. Similar implicit solutions were obtained for stiffness unbalanced joints.

Since the adherend just outside a single-lap joint is loaded both by the direct load P and the induced moment M_o, the average adherend stress can be much less than the maximum developed (adjacent to the bond line). The solution for balanced single-lap joints (Reference 3) is shown in Figure 26. Examination of Figure 26 shows that it is nearly impossible to design a single-lap joint strong enough to fail the weakest of adhesives in shear except by using an artificially short overlap. The failures actually observed for single-lap joints are shown in Figure 27. Figure 28 shows how adherend stiffness imbalance further reduces the low efficiencies of unsupported single-lap joints. The line $t_1/t_4 = 1$ represents the computations of Figure 26. The thinner adherend 1 is more severely loaded than is the thicker adherend 4.

Because the moment induced at the end of the overlap has such a dominant influence on joint efficiency, the behavior of single-lap joints differs markedly from that for double-lap joints. These moments are reduced towards zero as the overlap is increased, so increasing the overlap can significantly increase the joint strength.

Notwithstanding the dominant influence of the adherend rather than the adhesive on the strength of single-lap joints, and the inherently low joint efficiency, it is appropriate to analyze also for the shear stresses and peel stresses in the bond. The analysis for the elastic-plastic shear stress distribution (Reference 3) has been restricted to balanced joints here because of coupling between peel and shear stresses for unbalanced joints. Figure 29 shows the influence of adhesive plasticity on joint strengths for a representative

value of the eccentricity parameter. (The eccentricity in the load path results in the need to specify one more parameter than is necessary for double-lap joint solutions.) Figure 29 may be compared with Figure 11 for double-lap joints. Figure 30 shows the influence of the joint eccentricity on the potential bond shear strength for a specific degree of adhesive plasticity, showing how lesser eccentricities (thinner adherends) are associated with higher joint strengths. Just as with the influence of the adherend properties on single-lap joint strengths, the "plateau" strengths are not attained by overlaps of practical length and increasing the overlap increases the efficiency of the joint.

Figure 31 compares predictions for aluminum and steel adherends, all 1.5mm (0.060 inch) thick, for a common ductile adhesive. The greater Young's modulus of the steel increases the potential bond shear strength for a common overlap. Thus for this reason, as well as the greater adherend load necessary to cause yielding of the stronger stiffer metals, adhesives have been thought to be "stronger" when bonding steel or titanium than for aluminum. Experimental results of Reference 12 are compared with elastic-plastic single-lap joint theory in Figure 32. While the adhesive was found to be broken cohesively in every case (due largely to secondary failure after adherend yielding) every single failure not governed by the short overlap (fully plastic) criteria is bounded between the appropriate adherend yield and ultimate strength characteristics. In other words, all "long-overlap" failures were induced by the adherend and not the adhesive. Any influence of adhesive ductility is necessarily confined to establishing whether the failure occurs near the yield line (for brittle adhesives) or near the ultimate strength line (very ductile adhesives). The experimental results of Reference 12 given in Figure 33 show how a thicker adherend of the same material appears to "strengthen" an adhesive. With but one exception, data on composites (Reference 10) shown in Figure 34 appears to be explained by primary failure in the adherends arising from the combination of uniform and bending loads.

Due to the above effects analysts are cautioned against trying to interpret single-lap test data in the light of adhesive instead of adherend phenomena.

While the inclusion of adhesive plasticity in shear has increased the predicted bond strengths above the laminate strengths for thin and moderately thick

adherends, the low interlaminar tension strength of composite laminates renders peel stresses a problem for single-lap joints of thick adherends.

Based on the simplifying assumption that the adhesive shear stress is uniform, the present theory (Reference 3) predicts that the maximum peel stress is related to the average adherend tensile stress outside the joint by the relation

$$\frac{\sigma_p}{\sigma_{avg}} = \frac{k}{\sqrt{2}}\left(\frac{3E_c' t_1}{En}\right)^{\frac{1}{2}} , \tag{12}$$

where

$$k = 2M_o / Pt \tag{13}$$

is the moment coefficient deduced from the adherend analysis (Reference 3) of the eccentric loadpath. The same peel stress coefficient (quantity in parentheses) appears in both equations (10) for double-lap, and (12) for single-lap joints, but to different powers. The theory predicts a more powerful peel stress effect for single-lap joints. Figure 35 shows the equation (12) solution in which the coefficient k is determined as a function of the non-dimensionalized joint overlap by equation (11). High peel stiffnesses and short overlaps result in critical peel stress conditions. Increasing the overlap alleviates the problem because of the reduction in bending moment M_o. An expression similar in form to equation (12) has been programmed for unbalanced joints, which requires an iterative solution. Typical computations, illustrated in Figure 36, show how stiffness imbalance between the adherends of a single-lap joint aggravates the peel stress problem.

A representative combination of the separate analyses in Reference 3 for adherend bending strength, adhesive shear strength and interlaminar tension (peel) is illustrated in Figure 37. The joint strength is shown as a function of adherend thickness for a family of ℓ/t ratios. The laminate strength is included for reference. Figure 37 shows how the three failure modes interact for graphite-epoxy laminates bonded together with a brittle adhesive. Adherend

failures are confined to the lower left corner, while adhesive shear failures are predicted for the upper right corner and interlaminer tension failures for the lower right corner. The computer program used in preparing Figure 37 is listed in Reference 3.

The foregoing results (and Reference 3) indicate that uniform single-lap joints have inherently low efficiency because the joint can never be as strong as the basic adherend (except for purely in-plane shear loading). They should not be used for primary structural joints unless attached to a moment-resistant support to nullify the effects of the eccentricity in the load path.

SCARF JOINTS

A simple design procedure for scarf joints which has been previously employed is to determine the adherend load and compute the minimum overlap necessary by dividing the load per unit width by the "uniform" shear stress allowable. This method is seriously inadequate, if the adherends are dissimilar (References 13 and 14), due to the actual gross variation of shear stress which exists over the joint length. There are also local stress concentrations in the bond near the ends of the overlap but these are so small that they are insignificant for any real adhesive.

A power series solution for scarf joints was derived in Reference 4, which employs a recurrence formula for high order terms, with the first two terms in the series being determined by boundary conditions. This solution is computed directly by a digital computer program and several hundred joints can be solved in a minute of computing time. Figure 38 identifies the notation and geometry used for the scarf joint analyses. Precisely the same non-dimensionalized parameters are found to govern the scarf joint as were determined earlier for double-lap and single-lap joints. Figures 39 and 40 illustrate the effect of adherend stiffness and thermal imbalances, respectively, for a purely-elastic analysis. It is seen in Figure 39 that the ratio of average shear stress to peak shear stress asymptotes towards the ratio of adherend stiffnesses for very long overlaps. Although not shown in the figure, the same result is obtained regardless of any thermal mismatch present. Figure 40 shows that thermal mismatch between adherends has reduced effects on either very long or very short overlaps but

has significant effects for intermediate values. Figure 41 illustrates the interaction of adherend stiffness and thermal imbalances, as well as the effect of load reversal on the joint strength. Curve F of Figure 41 shows how, for severe thermal mismatches between adherends, the joint strength is zero beyond a certain overlap just as predicted by a purely-plastic analysis. What is somewhat more surprising is that, beyond a further overlap, the joint strength starts increasing again. This latter behavior was not predicted by the fully-plastic analysis (Reference 13) and derives from the fact that the elastic adhesive carries a proportionally greater fraction of the load in a scarf joint than it does in lap joints. Like double-lap joints, the a priori identification of the more critical end is not always possible when both thermal and stiffness imbalances occur, so a check must be made at each end to identify which is more critical. For stiffness imbalance alone, the end from which the softer adherend extends is always more critical than the other. Figure 41 shows how, unlike uniform lap joints, the shear strength of scarf joints can increase indefinitely with overlap, so an adequate strength in excess of the adherend strength can always be found even for thick sections.

In addition to the perfectly elastic solutions, Reference 4 contains details of an elastic-plastic analysis using the model discussed above and the corresponding computer program which was developed. Figure 42 illustrates the effect of adhesive plasticity on the strength reductions arising from adherend stiffness imbalance. Figure 43 shows the influence of adherend thermal mismatch on the shear strength of scarf joints in the absence of stiffness imbalance. While scarf joints do suffer strength losses due to thermal mismatch, these losses are far less severe than for a lap joint between the same adherends. Likewise, peel stresses are critical for thick-adherend lap joints, but are negligible for practical scarf joints. Indeed, the present analysis ignores peel stresses for practical joints because of the necessarily small scarf angle. The analytically predicted interaction of adherend imbalances is still of much the same form as shown in Figure 41, even when adhesive plasticity is included, but the effects are less pronounced.

Because the scarf joint analysis is governed by a differential equation having variable coefficients instead of the linear ones for lap joints, the influence of overlap on the potential shear strength of the bonds is different.

Beyond the overlaps of practical interest, the average stress in the scarf joint bond asymptotes toward a fixed value determined by any adherend stiffness imbalance alone and independent of the amount of adhesive plasticity. This differs from both the double-lap and single-lap joint behaviors, which is not surprising in view of the distinct geometries. In view of this there appears to be no clear cut merits in favor of designing in terms of either average stress or joint strength.

Experimental results providing a comparison with the predictions of this elastic-plastic theory of scarf joints are to be found in Reference 15. Unfortunately, there are indications of shortcomings with some of the test specimens.

The scarf joint is mathematically the most difficult to solve analytically of all the standard joints. The governing differential equations do not possess standard closed-form integrals. However the elastic-plastic analysis of the scarf joint has led to an explicit lower-bound solution which proved to be within a few percent of the precise series solution for nearly all practical material and geometric combinations of interest for design. This approximate solution is unduly conservative only for negligible adhesive plasticity ($\gamma_p/\gamma_e < 0.5$), severe adherend stiffness imbalance ($ETR < 0.2$) or severe adherend thermal mismatch ($|CTHERM| < 2$). This approximate solution follows from solving

$$\psi = 1 - \frac{\left\{\frac{(1+ETR)(\gamma_p/\gamma_e)}{(\lambda\ell)^2} + \left[\frac{(1+ETR)\ CTHERM}{(\lambda\ell)} - (1-ETR)\right]\psi\right\}}{\left[(1-ETR) - \frac{(1+ETR)\ CTHERM}{(\lambda\ell)}\right]\ell n(1-\psi)} \tag{14}$$

for ψ by iteration and substituting the result into the expression

$$\frac{\tau_{av}}{\tau_p} = 1 - \frac{\left\{\frac{(1+ETR)(\gamma_p/\gamma_e)}{(\lambda\ell)} + \left[\frac{(1+ETR)\ CTHERM}{(\lambda\ell)} - (1-ETR)\right]\psi\right\}}{\ell n(1-\psi)} \tag{15}$$

Just as with the double-lap and single-lap joints, the critical end of the joint may not be identifiable by inspection, so certain simple additional checks must

be employed and the lesser value of (15) adopted. The subscripts 1 and 2 are interchanged when checking the respective ends of the joints.

The present formulation deals with the existence of zero, one or two plastic adhesives zones, as required by the particular combination of joint parameters. It is subject only to the one restriction that the scarf angle be small as a pre-requisite to ignoring the peel forces. The dominant parameter for scarf joints is adherend stiffness imbalance which, for sufficiently long overlaps, is predicted by the present analysis to overpower even the adhesive plasticity effect. This characteristic cannot be changed by a different representation of the adhesive nonlinearity, so the influence of the precise representation of adhesive nonlinearity may well be small.

The analyses above for scarf joints pertain to adhesive shear stresses and it is demonstrated that a small enough scarf angle can always be found to transfer the full adherend strength through the bond with an adequate margin. There is, of course, a potential problem with the adherend strength if the scarf angle is too small. Specifically, one adherend will fail if the scarf angle θ is so small that

$$\theta < \tau_p / F_u \quad , \tag{18}$$

(where F_u is the ultimate adherend stress in tension, compression, or shear, as appropriate) at the more critical end of the joint (identified by the adhesive shear stress analysis).

STEPPED-LAP JOINTS

Stepped-lap joints share features in common with both double-lap joints and scarf joints. The scarf joint represents the mathematical limiting case of a stepped-lap joint with an infinite number of steps. Within each step, the stepped-lap joint exhibits the high stress concentrations of uniform lap joints. Taken as a whole, however, it is free from the absolute strength limit beyond some thickness which limits the utility of the double-lap joint. Stepped-lap joints are superior to scarf joints for boron-epoxy because of the finite thickness of the boron filament while the reverse holds true for the very thin

graphite fibers. Also, stepped-lap joints have an inherently greater tolerance on assembly without significant loss of strength than do scarf joints, particularly in the case of four joints surrounding a panel.

The mathematical model used in the stepped-lap joint analysis is shown in Figure 44. This also shows the factors which have been included in the analysis. Other analyses are to be found in References 14 and 16. Peel stresses have been ignored because normal practice is to have the end steps sufficiently thin to eliminate such problems. The double-lap joint analysis serves to check on this aspect.

Figures 45 to 47 contain representative solutions obtained with the stepped-lap joint computer program developed in Reference 4. The respective adherends are $(0°/\pm45°/90°)$ HTS graphite-epoxy and 6Al-4V titanium. Both elastic and elastic-plastic solutions are presented for representative high strength brittle and ductile adhesives. The greater strength of the ductile adhesive is evident even at the elastic level and particularly so at ultimate load. Whereas, with a brittle adhesive, failure occurs in the adhesive at 65 percent of the load capacity of the adherends the ductile adhesive has a theoretical shear strength 56 percent stronger than the adherends. It is shown in Figure 47 that a critical design detail is the possible yielding of the end step of the titanium, which is a characteristic problem with stepped-lap joints. This is why the two end steps were deliverately made much shorter than the others.

The predictions of the theory with regard to the ductile adhesive have been confirmed experimentally for the joint design shown at the top of Figure 45. The failure observed experimentally was tension through the composite just beyond the end of the titanium. The failure load was 4 percent above expectations, presumably because the laminate was of better than average quality. Comparable tests were not run for the brittle adhesive.

The digital computer analysis program developed in Reference 4 can accommodate arbitrary properties and dimensions for each step. The reason for this is the provision of a capability to incorporate design changes to alleviate the most critical internal stress details. An example of the use of this program to optimize a stepped-lap joint is shown in Figure 48. The steps of reduced

length in the lower diagram relieve completely the yielding problem in the titanium and effect a 7 percent increase in the compressive strength, bringing it up to the strength of the laminate outside the joint. This was accomplished without significant loss in tensile strength. The program can be efficiently and effectively used as a design tool for bonded stepped-lap joints.

One characteristic of stepped-lap joints inherited from the governing equations of double-lap joints is that the load transferred is independent of step lengths for sufficiently great overlaps. Indeed, the internal adherend and adhesive stresses at the ends of each and every step are found by analysis to be independent of changes in step length to one, some, or all of the steps provided that the steps are sufficiently long to allow the development of an elastic trough in the shear stress distribution. The impact of this phenomenon on the design of such joints is that, if analysis shows the joint to have insufficient strength, it is necessary to increase the number of steps and to decrease the incremental step thicknesses to improve the shear strength. A mere increase in step lengths will usually not suffice.

PRACTICAL JOINTS

Not all practical adhesive-bonded joints fit precisely into one of the classical configurations discussed above. Reference 5 is devoted to some of these non-classical types and includes such structures as multi-cell torsion boxes with other than one-to-one load transfer in the joint. Emphasis is also placed upon the joint details of composite-reinforced metal structures and bonded metal reinforcement around bolt holes in filamentary composites. One of the non-classical joint configurations in widespread use is the adhesive-bonded doubler. A brief summary of the various practical joints detailed in Reference 5 is presented here.

Adhesive-Bonded Doublers

The characteristic critical detail of the usual one-sided bonded doubler construction is the combined direct and bending stress in the skin at the tip of the doubler. In order to minimize this, the doubler is usually made only approximately 60 percent as thick as the skin. The problem is analogous

to that of the limited efficiency of the adherends of single-lap joints and is governed by a similar analysis with a different set of boundary conditions. Figures 49 and 50 are non-dimensionalized solutions for the effective adherend efficiency of isotropic materials. The allowable stress level of the skin/doubler combination is obtained by multiplying the strength of the skin material by the efficiency factor from Figures 49 and 50 for the appropriate geometry and dividing by the combined thickness of the skin and doubler. It is shown that, by extending the doubler, the effective eccentricity of the structure can be reduced and the efficiency of the entire skin raised at the cost of a relatively small weight increase for the doubler. The effect of this has long been known. A generous doubler permits a lighter structure to be used for a given load than does an inadequate doubler.

Since generous faying surfaces are necessarily required for efficient doubler design, the bond stresses are usually not critical. Reference 5 contains details of the appropriate adhesive analyses which should be employed for thick sections.

Selective Reinforcement by Unidirectional Composites

Two design concepts for the selective reinforcement of metal structures by unidirectional composite material are shown in Figure 51. Each has its own critical joint detail in ensuring that the composite can be loaded up efficiently without failure of the bond. The appropriate governing analyses presented in Reference 5 cover both the infiltrated extrusions, which are usually of uniform cross section, and the bonded-on straps, which usually have tapered ends to alleviate the stress concentrations associated with the local load transfer. The analyses predict a size limit of about one quarter inch diameter for 450 K (350 °F) cured boron-epoxy infiltrated into aluminum extrusions. For the bonded scarf joint at the end of the reinforcement, the analysis establishes the importance of maintaining continuity of net extensional stiffness along the length of the joint. This usually requires significant build-up of the metal part in close proximity to the tapering of the ends of the composite reinforcement. The theory of Reference 5 also computes any residual stresses in the adherends due to the thermal mismatch. These can be important for fatigue life predictions.

Bonded Metal Reinforcement Around Bolt Holes in Composites

Where space limitations do not permit an entire bolt load to be reacted by bearing directly on a filamentary composite structure it is common practice to bond on a local metal doubler. Most of the bolt load is reached by bearing against such doublers from which the load is transferred to the composite part by shear in the adhesive layer. Figure 52 illustrates the kinds of analyses on this subject to be found in Reference 5. For a uniform thickness doubler, the optimum location of the bolt is shown to be precisely in the middle of the doubler. The adhesive strain concentrations are minimized by making doublers of the same net stiffness as that of the composite. Figure 52 compares the relative bond strengths for representative ductile and brittle adhesives and also includes the strength of the HTS graphite-epoxy adherends. This strength cut-off line corresponds to 20 layers, each 0.127mm (0.005 in.) thick, of 0° plies within the laminate. Beyond that number, the joint will be weaker than the adherend. The brittle adhesive is seen to be unsuitable for this application for temperatures representative of the environment of subsonic transport aircraft. Precisely the same shear load will be transferred if the inner edge of the doubler is tapered (and nothing else is altered) because the critical location in the adhesive is rendered less critical but the effective bond area remains the same. The main advantage of tapering the doublers is that it affords significant peel stress relief to be provided at the inner end, thereby enabling much thicker sections to have doublers bonded on effectively than would be possible with uniform doublers. In addition, slightly greater shear transfer capacity can be developed by careful design of the tapered doubler proportions. Tapered doublers on the outside of a laminate have proved to be more effective than those incorporated within the layup because the higher quality of the uniform laminate without joggles in the fibers more than makes up for the extra bond area of the internal doubler (see Figure 53).

In-Plane Shear Transfer Through Bonded Joints

Reference 5 presents an analysis technique for the in-plane shear transfer of a multi-cell torsion box as shown in Figure 54. In such a case, with multiple and parallel load paths, the analysis problem is compounded by the need

to distribute the bond shear loads in accordance with the respective stiffnesses of the various load paths. Coupled with this is the need to check each extremity of each bond area to identify the critical location. Then the associated loads developed in the non-critical bonds are less than their individual ultimate capacities. The design of such joints simply by summing the strengths of each part alone is shown to be unconservative.

The analysis of these joints serves to illustrate a powerful simple approximate analysis method developed for adhesive-bonded joints. This is the fully plastic analysis method. In this, the bond area is separated into narrow fully-effective strips around the periphery of a completely unloaded central zone. The widths of such strips are evaluated in terms of the elastic and plastic adhesive shear strains and the adherend properties. The load capacities of the joints then follow as the product of the effective bond area and the peak bond shear stress. This analytical method enables useful solutions to be obtained for quite complex joint geometries.

Peel Stress Relief for Double-Lap Joints

Reference 5 includes an approximate (fully-plastic) analysis of tapered double-lap joints which effectively relieve the peel stresses developed with uniform lap-joints by removing the hard point in the outer adherend under which the peak peel stresses were located. It is shown that by making the outer adherends 32.5* percent stiffer together than the inner adherend, the potential bond shear strength could be increased by 24 percent. The solution is illustrated in Figure 55 which shows the potential of this simple technique in bonded joint construction. The minimum overlaps shown, for one side of the double-strap joint, include an allowance for the elastic adhesive zone, but do not provide for manufacturing tolerances. Scarf and stepped-lap joints are far more expensive to fabricate than are uniform lap joints and the tapering of only the outer adherends permits the economies and ease of fit of uniform lap joints to be extended to a much greater thickness range than would otherwise be possible.

* It is interesting to note that this factor corresponds very closely with design practice for double-lap bolted joints with uniform inner adherends and scarfed outer adherends.

EFFECT OF SIZE ON SELECTION OF JOINT CONFIGURATION

The preceding analyses have established that, for all configurations except for the scarf and stepped-lap joints, there are inherent limitations on the strength developable by a given joint geometry. Beyond some thickness, the simpler joints are inadequate to load the structural members efficiently. Conversely, there is no point in using a more complex joint than is needed for joining thin adherends. This is shown graphically in Figure 56, based on the findings of the present investigation. This figure shows how, as the thickness of the structural members increases, it is necessary to change the basic configuration of the joint in order to maintain a joint strength at least as great as that of the adherends outside the joint.

CONCLUDING REMARKS

This report has summarized the development and application of elastic-plastic bonded joint analysis. This method has provided insight into the basic phenomena governing bonded joint behavior. It has led to design techniques accounting for the major parameters affecting joint behavior, in some cases for the first time. All of the standard joint classes, the double-lap, single-lap, stepped-lap, and scarf joints, have been analyzed and solutions presented. Adhesive plasticity, adherend stiffness imbalance and adherend thermal mismatch are considered. The theoretical predictions have been shown to be in agreement with the experimental evidence.

The analyses indicate that, for thin adherends, the bond shear strength is usually so far in excess of the adherend strength that joint design is easily accomplished. For somewhat thicker sections, the adherend strength increases more rapidly than the bond shear strength, indicating that lap-joint efficiency may be limited. For still thicker sections, particularly with filamentary composites, peel stress failures dominate and stress concentration relief techniques are needed to make lap joints effective. For still thicker sections yet, scarf or stepped-lap joints are needed.

In addition, most of the present analyses have shown an insensitivity to the precise form of adhesive characterization, the adhesive influence being determined specifically and uniquely by the strain energy in shear.

APPENDIX A

PRACTICAL DESIGN CONSIDERATIONS

The analyses above have identified a variety of stress concentration details within bonded joints. With a thorough understanding of such problem areas, in conjunction with accumulated practical experience, it becomes possible to alleviate potential weaknesses. Some such improvements, such as the peel-stress relief of double-lap joints by tapering the outer adherends, have been discussed in the body of the report. Others are described briefly here.

The inefficiency of unsupported single-lap joints arises from the eccentricity in the load path. When supported on moment-resistant restraints, as per standard aircraft construction practice, the eccentricity is nullified and the efficiency increased. Figure 57 illustrates such an application, with a heavy flange providing the support. The joint load capacity then approaches one-half of the equivalent double-lap (back-to-back) joint. This same illustration explains also how suitably-designed bonded-bolted joints are quite efficient. While the static load transferred may not greatly exceed that of the bond alone, the mechanical fasteners serve as tooling aids, fail-safe load paths, and crack arrestors to stop the spread of any local delamination of the bond.

One technique for improving the overall structural efficiency of single-lap joints that is particularly suited to filamentary composite laminates is shown in Figure 58. The integral build-up shown is easily accomplished during composite fabrication. A scheme for selecting the matching thicknesses is discussed in Reference 3.

The analysis presented for scarf joints between dissimilar materials demonstrated how adherend thermal mismatch weakens scarf joints throughout the range of lengths which are usually of practical interest. A known design modification, the multiple saw-toothed scarf of Figure 59, alleviates this problem by combining the less severe thermal mismatch effects from shorter overlaps with a great increase in bond area otherwise not obtainable except by going to an impractically long single overlap. This same overlapping technique is favorable for reducing stiffness imbalance effects also. The alternative of longer

overlaps to alleviate thermal problems generally worsens, and never improves, the stiffness imbalance effects.

Figure 60 illustrates two practical techniques for overcoming the adherend tip fracture problem for scarf joints. The analysis indicates that the tip of the stiffer adherend is a probable high stress location. The schemes suggested have been found to work in practice. It has been found impractical to fabricate a scarf with a tip much less than 0.25 to 0.37 mm (0.010 to 0.015 inch) thick due to machining difficulties. The extension of the adhesive beyond the end of the scarf in the lower illustration is intended to unload the cut fibers more gradually than would be the case if the composite resin were used for that purpose. It will be observed that a key feature of the schemes is that no net section reduction of the composite is suffered at the right hand ends of the joints shown in Figure 60. As explained by the analysis, the total extensional stiffness of the two adherends should be maintained constant at all stations along the joint in order to maximize the joint efficiency.

Care should be exercised in the design of stepped-lap joints not to weaken the adherend unduly at the edge of the joint by a reduction in net section at the first step, as is explained in Figure 61.

APPENDIX B

SCALING EFFECTS IN BONDED JOINTS

There is an inherent deficiency in the testing of subscale bonded joints for design concept verification. Were one able to scale precisely, up or down, absolutely all of joint dimensions, the non-dimensionalized joint parameters would remain constant as also would the average shear stress. In practice, however, the adhesive thickness is held constant at about 0.13 to 0.25 mm (0.005 to 0.01 inch) regardless of the overall joint size because the quality of the bond deteriorates with the voids usually formed in thick bond lines and because of the unavailability of extra thin adhesive films for test purposes. The present analyses indicate that the adhesive layer thickness always occurs as a product with the adhesive shear strain on thick bond lines. Thus, in scaling up all joint dimensions except the adhesive layer thickness, the non-dimensionalized joint parameters are altered in the direction of aggravating the stress and strain concentrations in the bond or the adjacent adherend. The effect of neglecting these scaling considerations is shown in Figure 62. Each of the joint configurations shown is drawn to the same scale. One starts with the double-lap joint at A which performs satisfactorily for the size shown. By doubling the size of the joint one might have expected to attain the load at C. Based both on test experience (Reference 18) and the predictions of the present analysis of the internal stress distribution within the joint, one would actually realize the lower load at B. To efficiently load that greater thickness of adherend would require the tapered-lap shown for C. In scaling up this tapered-lap configuration without accounting for the non-uniform bond stress distribution one would have expected to develop the strength at E. The actual strength developed would be only as high as D. To develop the load at E, one would need the scarf (or stepped-lap) joint shown. The present analysis method provides the capability of accounting for the actual internal stress distribution within a bonded joint. In an older method of relying on a fictitious allowable bond shear stress, the allowable was not a material property at all and varied with the joint configuration as well as with the dimensions. Neither could the design allowable concept account for the failures induced by peel stresses which are now recognized as the

primary cause of failure for most uniform lap joints. These previously unexplained scaling phenomena (see Reference 18) are now seen to be quite simply the consequence of maintaining a constant bond-line thickness with joints of different size.

APPENDIX C

SURFACE PREPARATIONS FOR ADHESIVE BONDING

The durability of adhesive bonded joints depends primarily on the surface preparation for both metal and composite adherends. It is the interface between the adhesive and adherend that is more prone to environmental degradation than either the adhesive or adherends alone. For this reason, the problem of surface preparation for bonding continues to warrant attention. Bond failures within a joint can occur in two basic modes. The stronger failure mode is a cohesive failure of the adhesive. Surface preparation and processing leading to this behavior are considered desirable. The inherently weaker failure mode is due to poor adhesion at the adhesive-to-adherend interface and is not necessarily associated with contamination prior to bonding. Attack of the adhesive-to-metal interface by moisture has been a real problem in bonded joints, even with the standard chromic-acid etch for aluminum. The bonding of titanium remains a particularly difficult task. Such adhesion failures also occur with bonding of composites and are undesirable for three important reasons. Firstly, the surface phenomena are not governed by characteristic material properties and the strength level attained is dependent on the skill of the operator and decreases under environmental attack. Secondly, as a result of this, more reliance must be placed on empirical test data for the actual geometry under investigation because the scaling factors cannot be determined analytically since all of the solutions developed for bonded joints pertain to cohesive failures. This extra testing is both expensive and time-consuming. Thirdly, such joints are so weak that it is usually not possible to develop adequate joint efficiency. Since it is the interface which is more prone to environmental degradation than either the adhesive or adherend, it is imperative to establish surface preparations which consistently develop cohesive bond failures. Cured epoxy composite matrices are relatively inert and special treatments are necessary to enhance the bond to the adhesive. Tests were performed because the theory described here had predicted that a substantial strength increase was available, for graphite/epoxy-to-graphite/epoxy bonded joints, beyond the then current strengths as shown in Figure 63. In this case, theory preceeded and guided

experiment to a major improvement in joint strength and reliability. The strength increase achieved by grit-blasting the surface prior to bonding is illustrated in Figure 64. More important than the absolute strength values is the change in failure mode. Additional improved surface preparations have been developed since but more work remains to be done in the field of optimum surface preparation for production.

REFERENCES

1. Hart-Smith, L. J., "Design and Analysis of Adhesive-Bonded Joints," Douglas Aircraft Company, Paper No. 6059A, presented to Air Force Conference on Fibrous Composites in Flight Vehicle Design, Dayton, September 1972.

2. Hart-Smith, L. J., "Adhesive-Bonded Double-Lap Joints," NASA CR-112235, January 1973.

3. Hart-Smith, L. J., "Adhesive-Bonded Single-Lap Joints," NASA CR-112236, January 1973.

4. Hart-Smith, L. J., "Adhesive-Bonded Scarf and Stepped-Lap Joints," NASA CR-112237, January 1973.

5. Hart-Smith, L. J., "Non-Classical Adhesive-Bonded Joints in Practical Aerospace Production," NASA CR-112238, January 1973.

6. Gehring, R. W., Matoi, T. T., and Hughes, E. J., "Evaluation of Environmental and Service Conditions on Filamentary Reinforced Composite Structural Joints and Attachments," AFML-TR-71-194, Vol I, pp 172-179, November 1971.

7. Volkersen, O., "Die Nietkraftverteilung in Zugbeanspruchten Nietverbindungen mit Konstanten Laschenquerschnitten," Luftfahrtforschung 15, 4-47 (1938).

8. de Bruyne, N. A., "The Strength of Glued Joints," Aircraft Engineering, 16, 115-118, 140 (1944).

9. Oken, S. and June, R. R., "Analytical and Experimental Investigation of Aircraft Metal Structures Reinforced with Filamentary Composites," NASA CR-1859, 1971.

10. Lehman, G. M., Hawley, A. V., et al, "Investigation of Joints in Advanced Fibrous Composites for Aircraft Structures," AFFDL-TR-69-43, Vols. I & II, June 1969.

11. Goland, M. and Reissner, E., "The Stresses in Cemented Joints," J. Appl. Mech. 11, A17-A27 (1944).

12. Wegman, R. F. and Devine, A.T., "Adherend Mechanical Properties Limit Adhesive Bond Strengths," SAMPE 14th National Symposium Proceedings, Florida, Paper No. 1-4-2, November 1968.

13. Sumida, P. T., Hart-Smith, L. J., Pride, R. A., and Illg, W., "Filamentary Composite REinforcement of Metal Structures," SPI 28th Annual Western Conference Proceedings, San Diego, 74-90, May 1971.

14. Erdogan, F., and Ratwani, M., "Stress Distribution in Bonded Joints," J. Composite Materials 5, 378-393 (1971).

15. Lackman, L. J., Arvin, G. H., et al., USAF, "Structural Design Guide for Advanced Composite Applications," Volume II, Analytical Methods, Second Edition, January 1971.

16. Grimes, G. C., Wah, T., et al, "The Development of Nonlinear Analysis Methods for Bonded Joints in Advanced Filamentary Composite Structures," AFFDL-TR-72-97, September 1972.

17. Reed, D. L. and Rogers, C. W., "Design Criteria," 18th National SAMPE Symposium, Los Angeles, pp 23-34, April 1973.

TABLE 1. - TYPICAL ROOM-TEMPERATURE ADHESIVE CHARACTERISTICS

ADHESIVE TYPE	MAXIMUM BOND SHEAR STRESS	MAXIMUM BOND-LINE DISPLACEMENT [NOMINAL ADHESIVE THICKNESS 0.127 mm (0.005 in.)]
Unplasticized adhesives [450 K (350°F) cure]	55-69 (MN/m^2) 8-10,000 (psi)	0.013-0.051 (mm) 0.0005-0.002 (in.)
Plasticized adhesives [450 K (350°F) cure]	41-55 (MN/m^2) 6-8,000 (psi)	0.25-0.76 (mm) 0.010-0.030 (in.)
Plasticized adhesives [394 K (250°F) cure]	28-41 (MN/m^2) 4-6,000 (psi)	0.25-0.51 (mm) 0.010-0.020 (in.)

TABLE 2. - MATERIAL PROPERTIES FOR FIGURES 23, 24 AND 55

7075-T6 ALUMINUM ALLOY:

$E = 71$ GN/m^2 (10.3×10^6 psi),

$F_{ty} = 483$ MN/m^2 (70 ksi), $F_{tu} = 552$ MN/m^2 (80 ksi).

HIGH-STRENGTH GRAPHITE-EPOXY:

$(0°/+45°/90°/-45°)_s$ pattern:

$E_L^t = 55$ GN/m^2 (8.0×10^6 psi), $E_N^t = 12$ GN/m^2 (1.7×10^6 psi),

$F_L^{tu} = 476$ MN/m^2 (69 ksi), $F_N^{tu} = 55$ MN/m^2 (8 ksi),

$(0°/+45°/0°/-45°)_s$ pattern:

$E_L^t = 82$ GN/m^2 (11.9×10^6 psi), $E_N^t = 12$ GN/m^2 (1.7×10^6 psi),

$F_L^{tu} = 710$ MN/m^2 (103 ksi), $F_N^{tu} = 55$ MN/m^2 (8 ksi),

(0°) unidirectional laminate:

$E_L^t = 145$ GN/m^2 (21.0×10^6 psi), $E_N^t = 12$ GN/m^2 (1.7×10^6 psi),

$F_L^{tu} = 124$ MN/m^2 (180 ksi), $F_N^{tu} = 55$ MN/m^2 (8 ksi),

(in which the subscript N refers to properties in the thickness direction).

DUCTILE ADHESIVE:

$\tau_p = 41.4$ MN/m^2 (6 ksi), $\eta = 0.13$ mm (0.005 in.), $\gamma_p/\gamma_e = 20$,

$\eta(\frac{1}{2}\gamma_e + \gamma_p) = 0.259$ mm (0.0102 in.), $E_c \simeq 3.45$ GN/m^2 (500 ksi),

$\sigma_{c_{max}} \simeq 69$ MN/m^2 (10 ksi).

BRITTLE ADHESIVE:

$\tau_p = 62.1$ MN/m^2 (9 ksi), $\eta = 0.13$ mm (0.005 in.), $\gamma_p/\gamma_e = 1.5$,

$\eta(\frac{1}{2}\gamma_e + \gamma_p) = 0.011$ mm (0.00042 in.), $E_c \simeq 10.35$ GN/m^2 (1500 ksi),

$\sigma_{c_{max}} \simeq 117$ MN/m^2 (17 ksi).

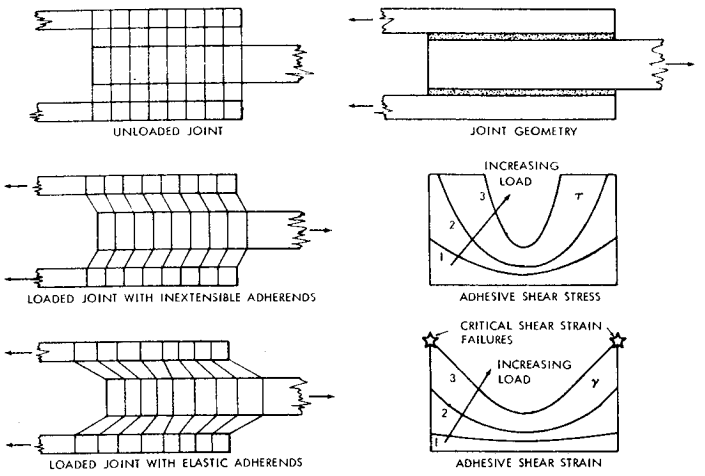

FIGURE 1. SCHEMATIC EXPLANATION OF SHEARING IN ADHESIVE

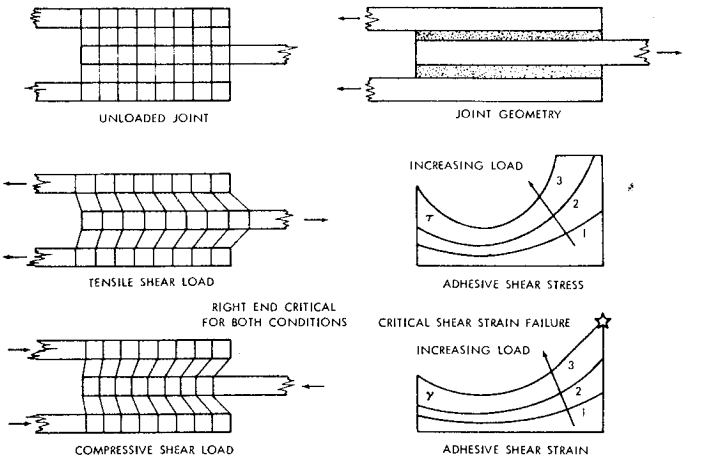

FIGURE 2. DEFORMATIONS AND ADHESIVE STRAINS IN STIFFNESS-UNBALANCED BONDED JOINTS

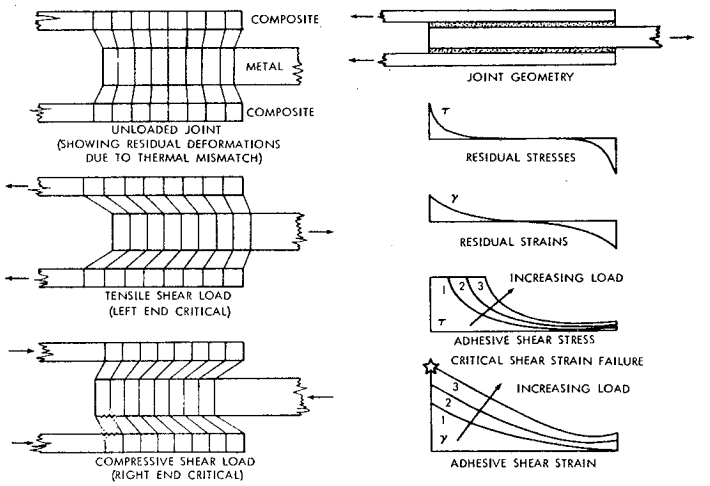

FIGURE 3. DEFORMATIONS AND ADHESIVE STRAINS IN THERMALLY-MISMATCHED BONDED JOINTS

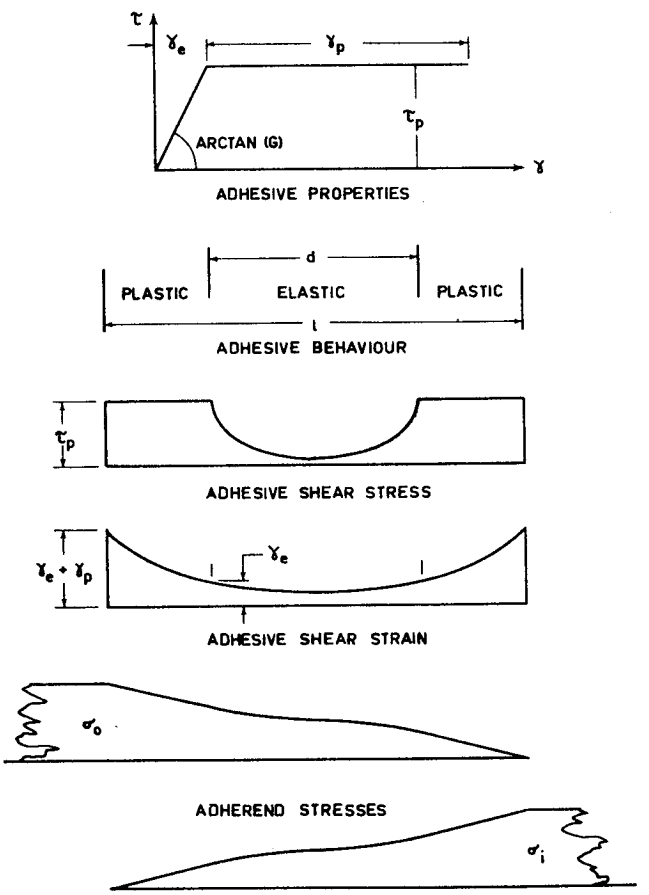

FIGURE 4. STRESSES AND STRAINS IN DOUBLE-LAP BONDED JOINTS

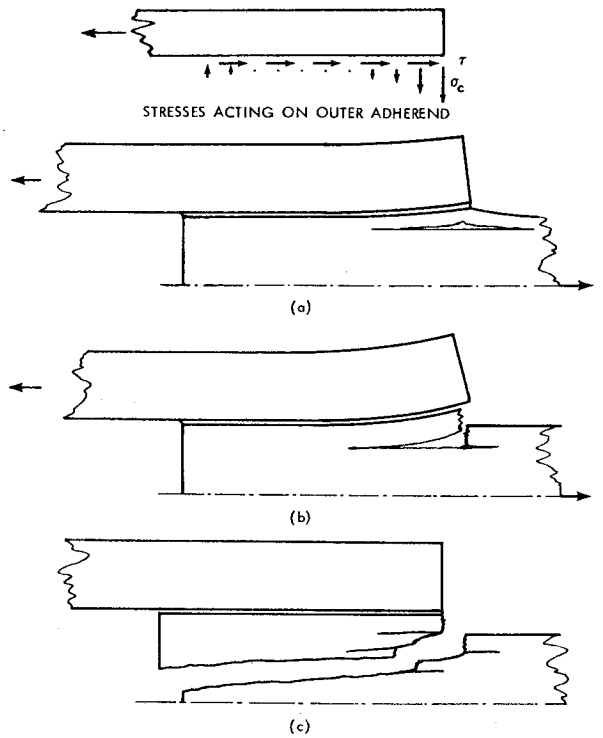

(a), (b), (c) INDICATE FAILURE SEQUENCE

FAILURE IS NORMALLY IN CENTRAL ADHEREND, RATHER THAN OUTER ADHEREND(S), BECAUSE OF HIGHER IN-PLANE STRESSES

FIGURE 5. PEEL-STRESS FAILURE OF THICK COMPOSITE JOINTS

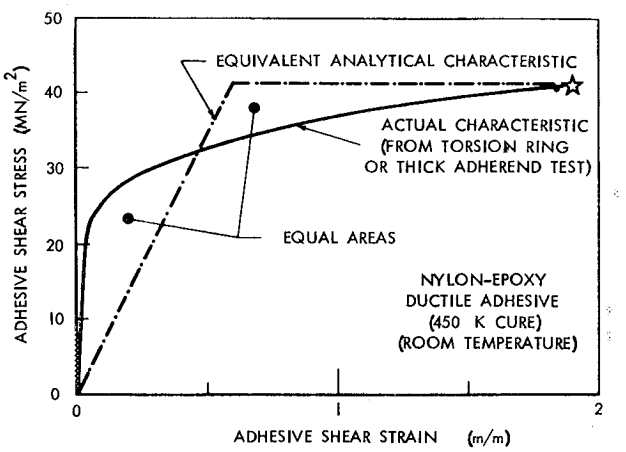

FIGURE 6. ELASTIC-PLASTIC REPRESENTATION OF ACTUAL ADHESIVE SHEAR CHARACTERISTICS

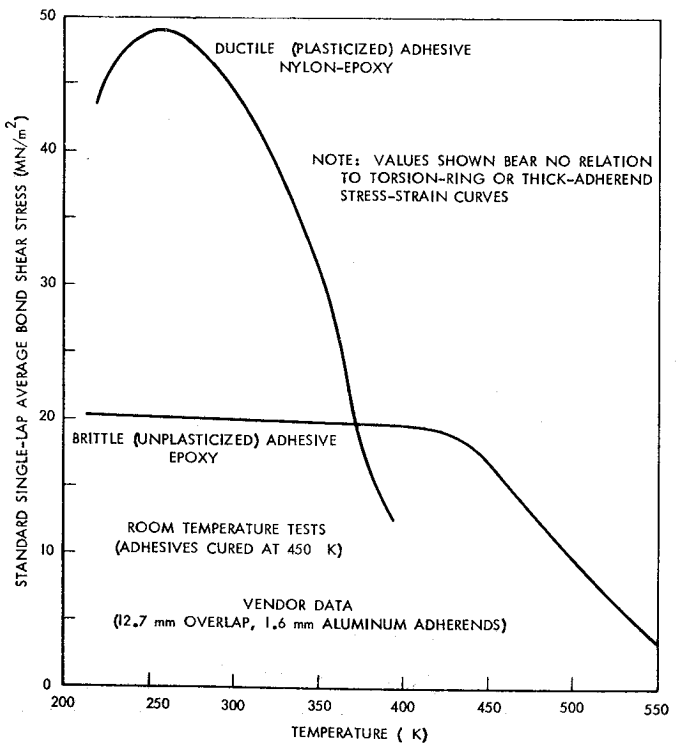

FIGURE 7. COMPARISON OF DUCTILE AND BRITTLE ADHESIVE STRENGTHS AT VARIOUS TEMPERATURES

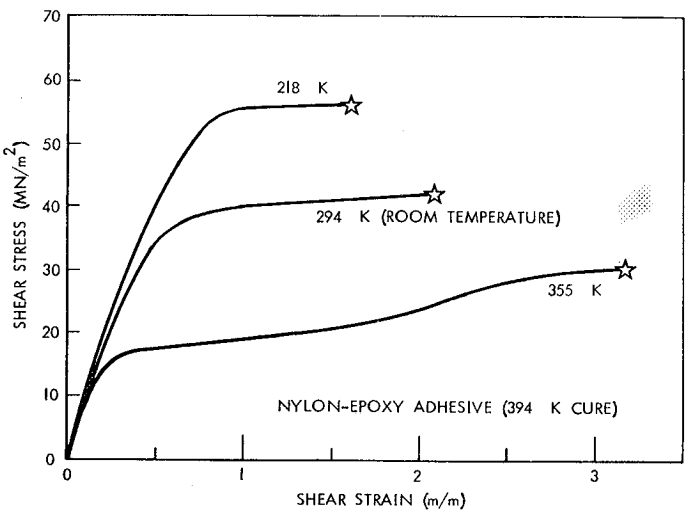

FIGURE 8. STRESS-STRAIN CHARACTERISTICS OF ADHESIVE FILM IN SHEAR, SHOWING TEMPERATURE DEPENDENCE

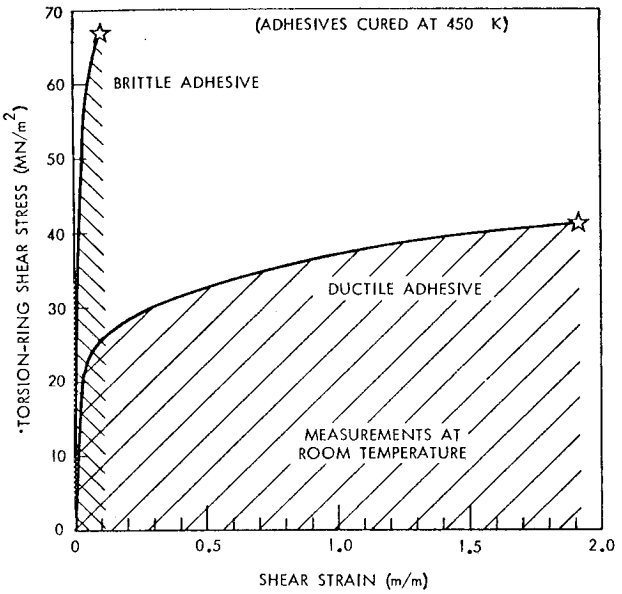

FIGURE 9. COMPARISON OF SHEAR STRESS-STRAIN CHARACTERISTICS FOR BRITTLE AND DUCTILE ADHESIVES

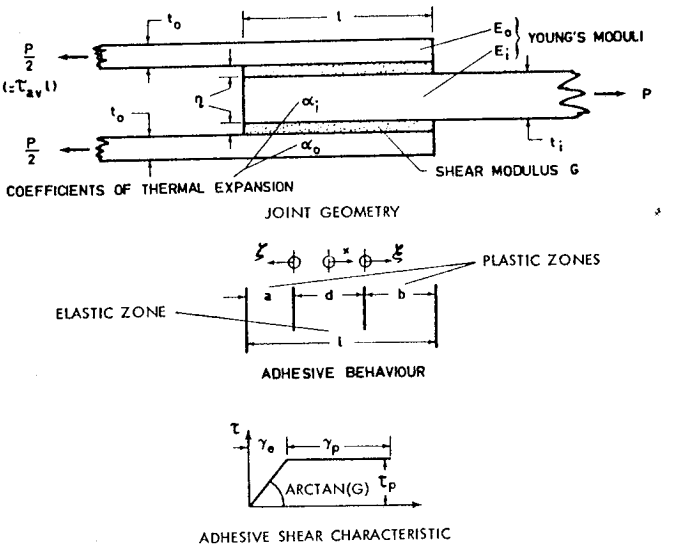

FIGURE 10. GEOMETRY OF A DOUBLE-LAP BONDED JOINT (DISSIMILAR ADHERENDS)

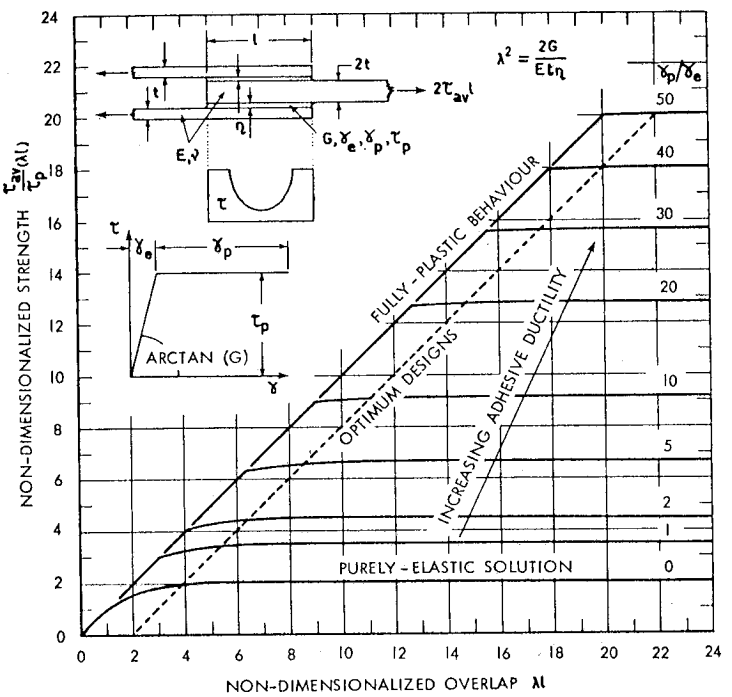

FIGURE 11. SHEAR STRENGTH OF BALANCED DOUBLE-LAP BONDED JOINTS

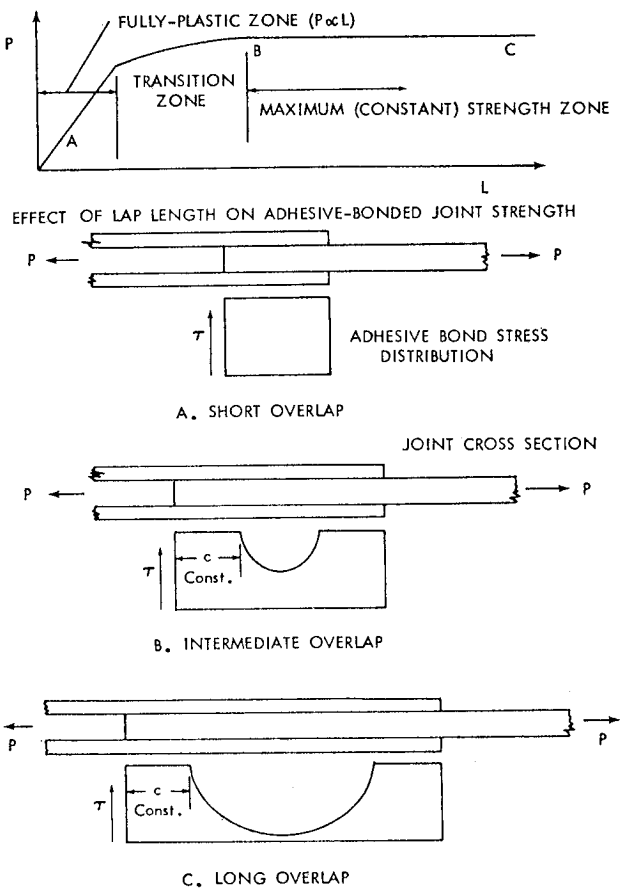

FIGURE 12. INFLUENCE OF LAP LENGTH ON BOND STRESS DISTRIBUTION

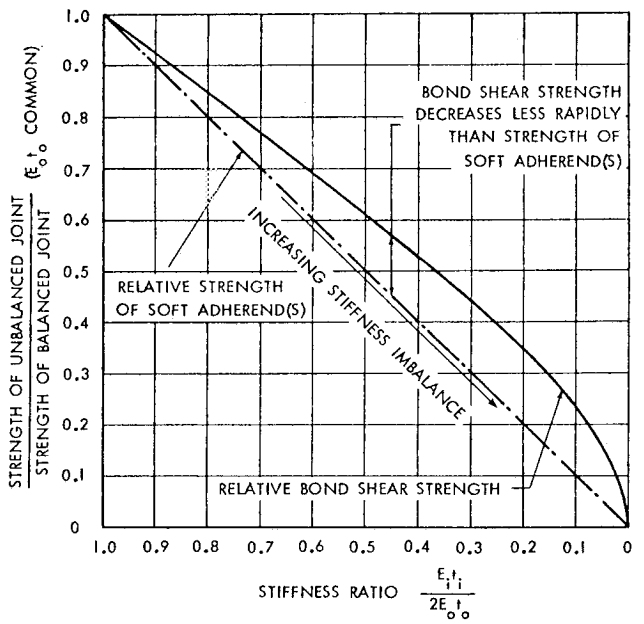

FIGURE 13. STRENGTH REDUCTION FACTOR IN DOUBLE-LAP BONDED JOINTS, DUE TO ADHEREND STIFFNESS IMBALANCE

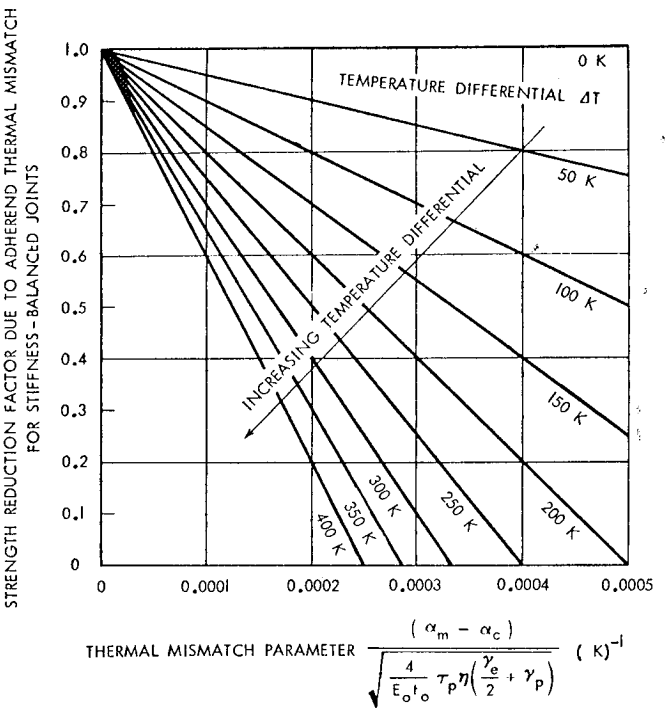

FIGURE 14. STRENGTH REDUCTION FACTOR IN DOUBLE-LAP JOINTS, DUE TO ADHEREND THERMAL MISMATCH

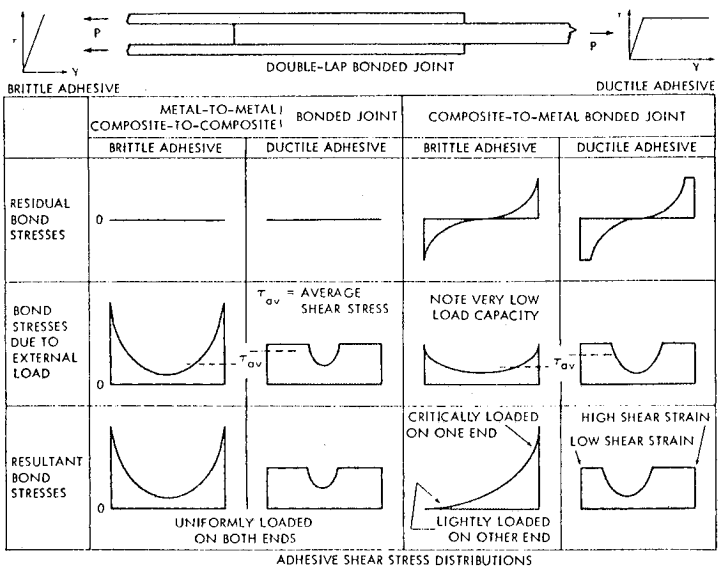

FIGURE 15. ADHESIVE SHEAR STRESS DISTRIBUTIONS IN METAL-TO-COMPOSITE JOINTS (COMPARISON OF BEHAVIOR OF BRITTLE AND DUCTILE ADHESIVES)

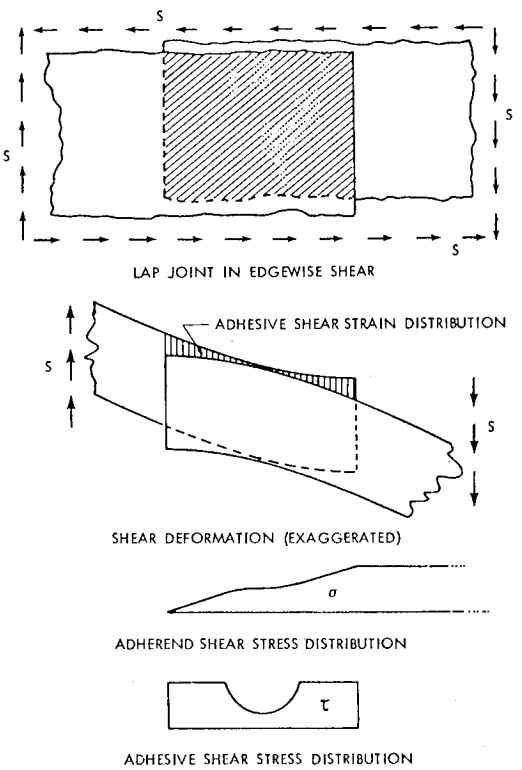

FIGURE 16. ADHESIVE-BONDED JOINT LOADED BY IN-PLANE (EDGEWISE) SHEAR

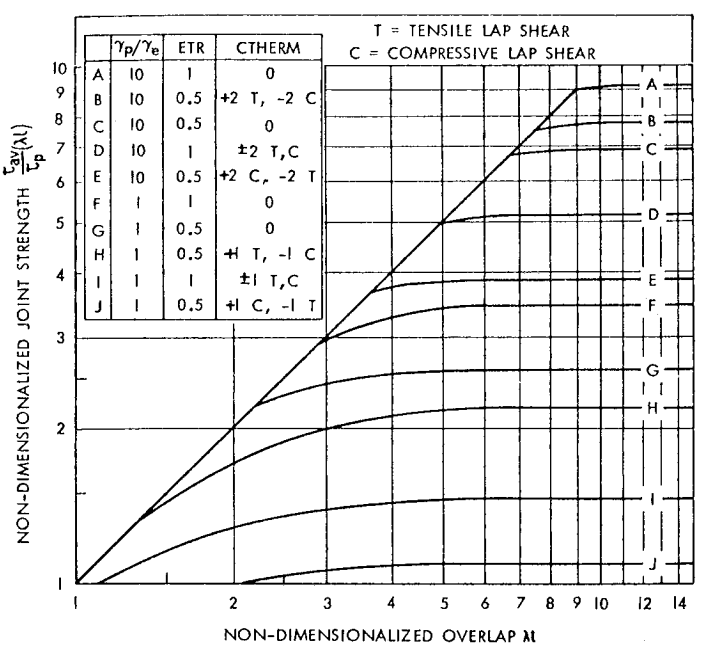

FIGURE 17. EFFECT OF LOAD REVERSAL ON STRENGTH OF UNBALANCED DOUBLE-LAP BONDED JOINTS

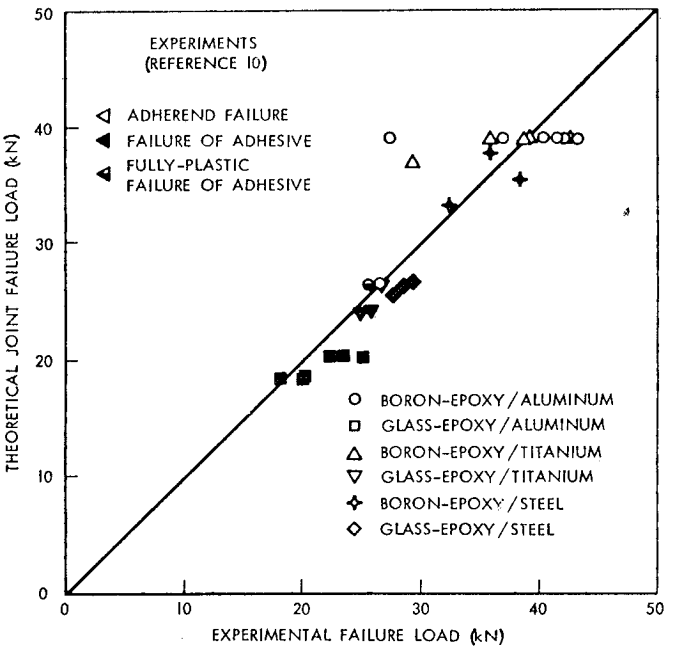

FIGURE 18. COMPARISON BETWEEN THEORY AND EXPERIMENT FOR DOUBLE-LAP BONDED JOINTS

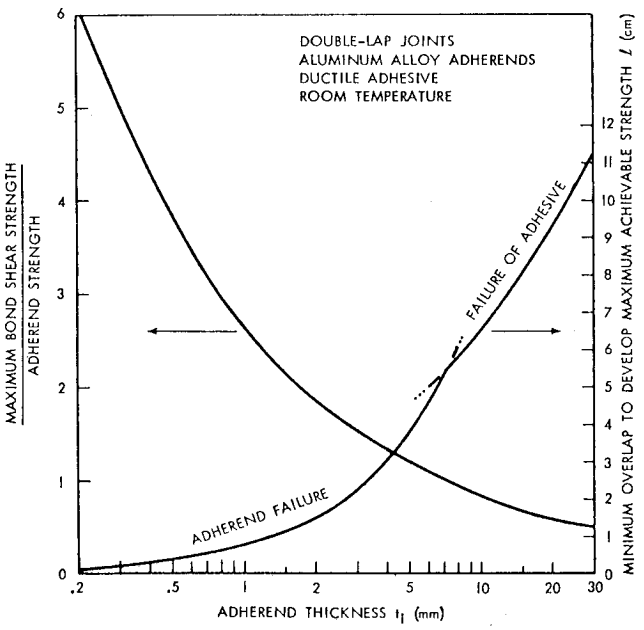

FIGURE 19. THEORETICAL BOND STRENGTHS AND MINIMUM OVERLAPS FOR DOUBLE-LAP BONDED JOINTS

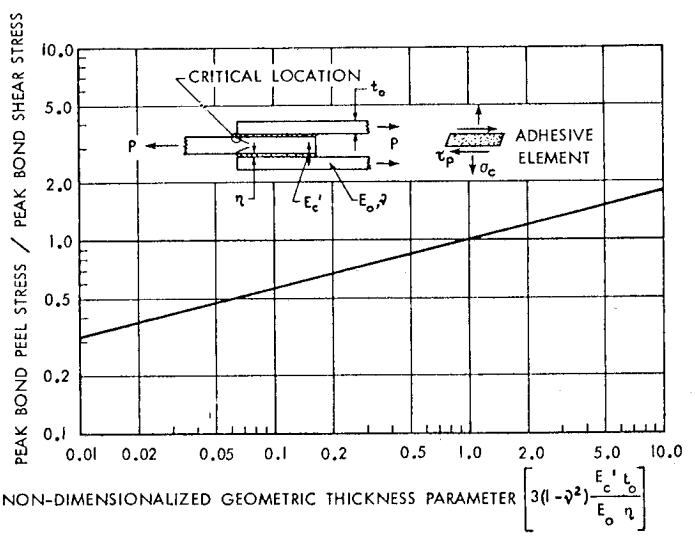

FIGURE 20. PEEL STRESSES IN DOUBLE-LAP BONDED JOINTS

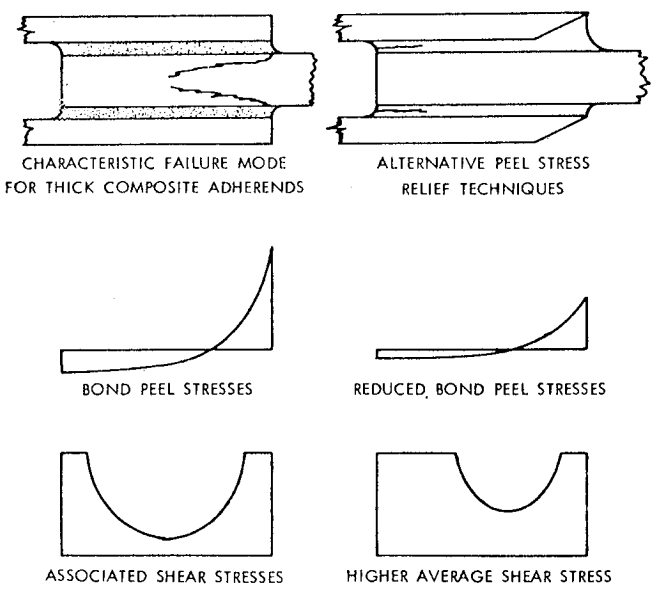

FIGURE 21. RELIEF OF PEEL STRESS FAILURE OF THICK COMPOSITE BONDED JOINTS

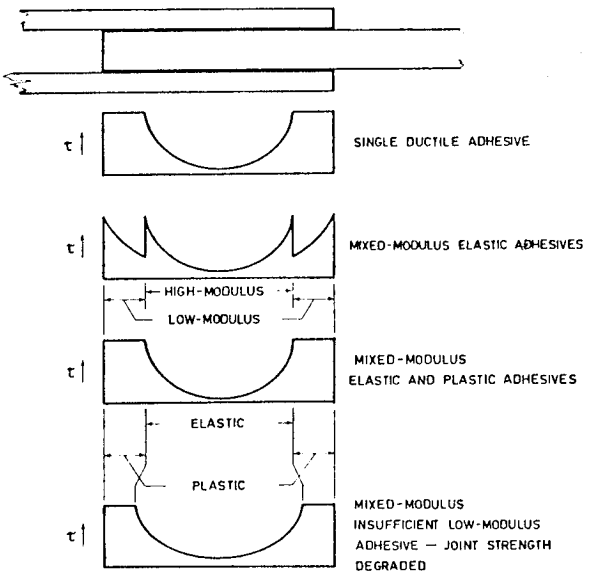

FIGURE 22. MIXED MODULUS ADHESIVE JOINTS (SHEAR STRESS DISTRIBUTIONS)

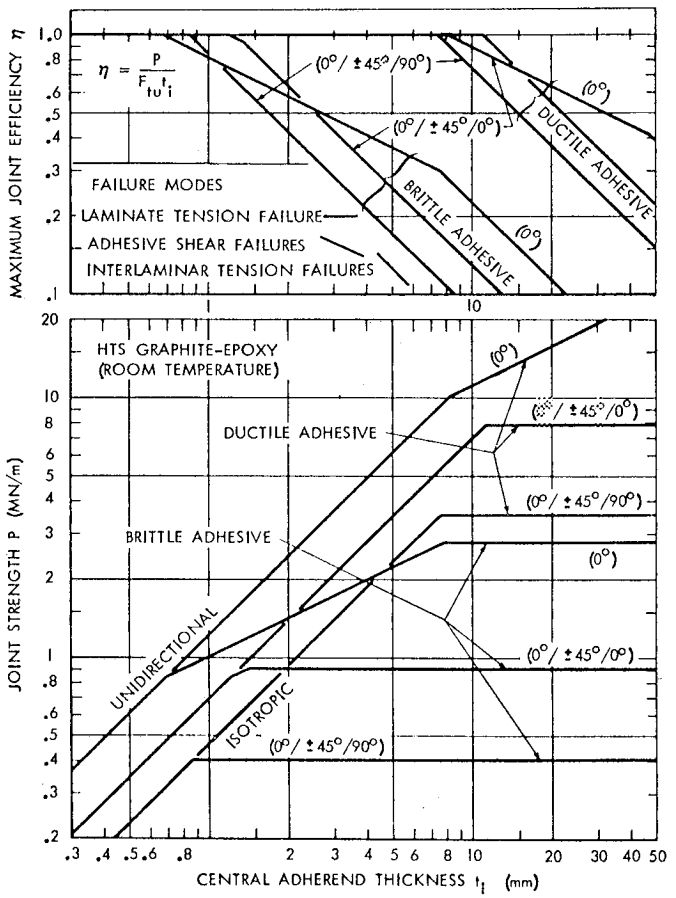

FIGURE 23. MAXIMUM EFFICIENCY AND JOINT STRENGTHS FOR GRAPHITE-EPOXY DOUBLE-LAP JOINTS

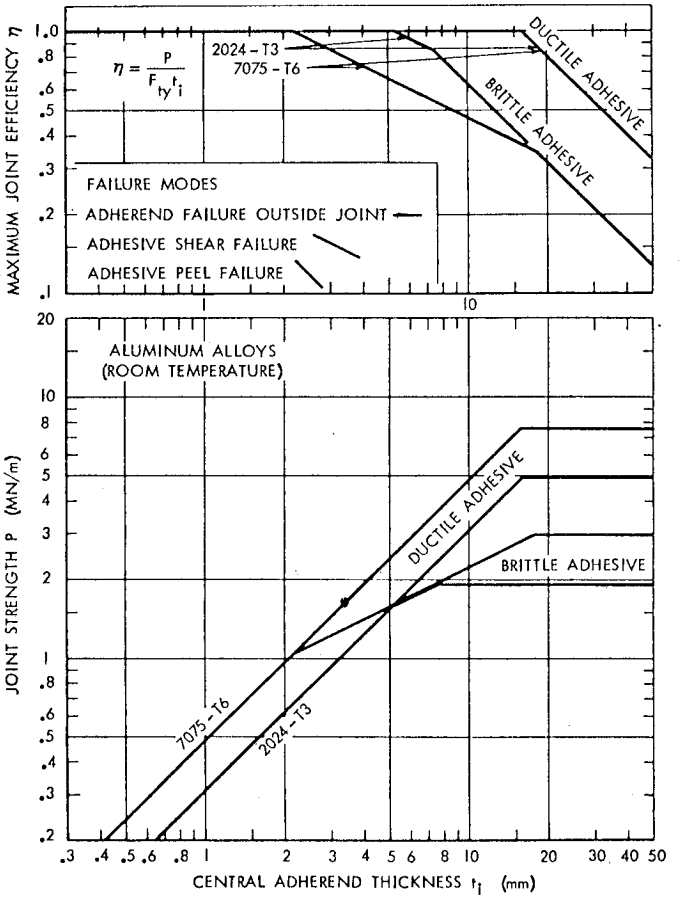

FIGURE 24. MAXIMUM EFFICIENCY AND JOINT STRENGTHS FOR ALUMINUM DOUBLE-LAP JOINTS

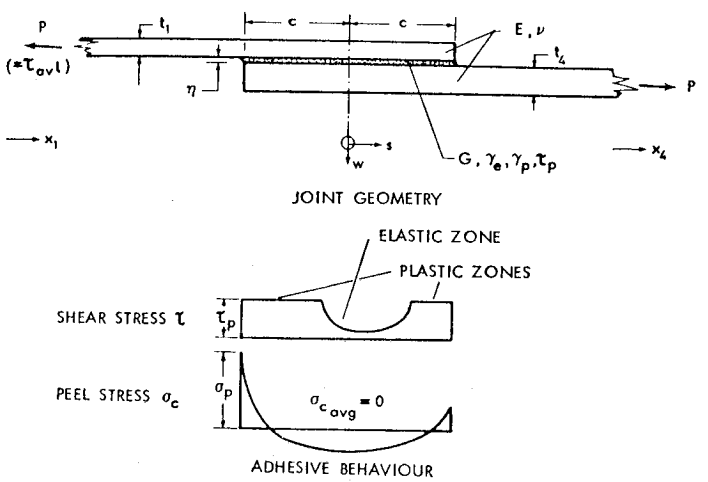

FIGURE 25. GEOMETRY AND BOND STRESS CHARACTERISTICS IN SINGLE-LAP JOINTS

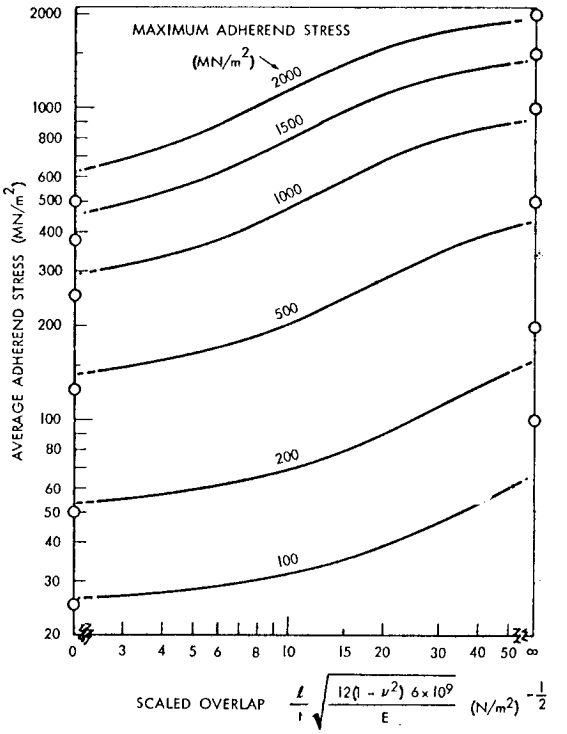

FIGURE 26. ADHEREND LIMIT LOADS FOR SINGLE-LAP BONDED JOINTS

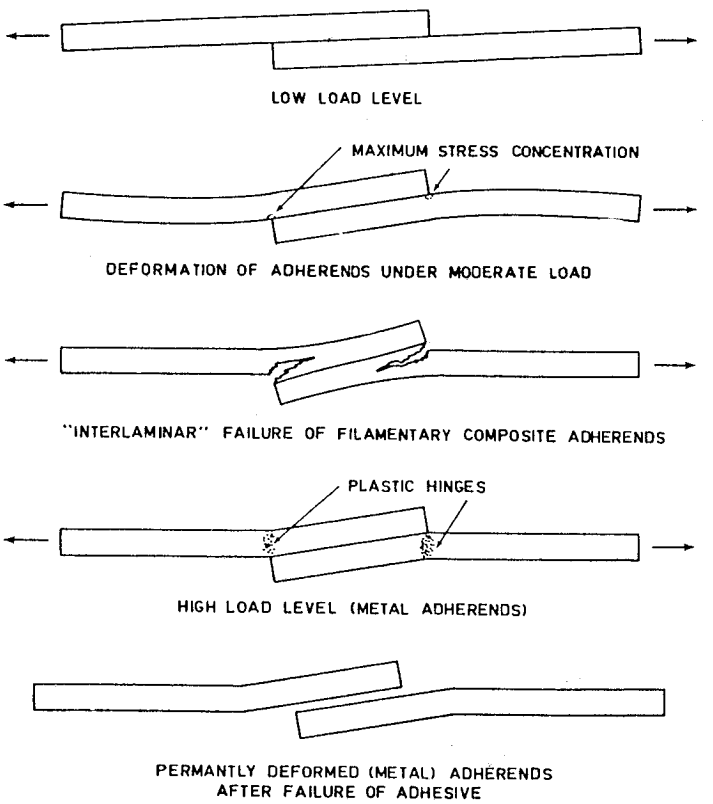

FIGURE 27. FAILURE OF SINGLE-LAP BONDED JOINTS WITH BRITTLE AND YIELDING ADHERENDS

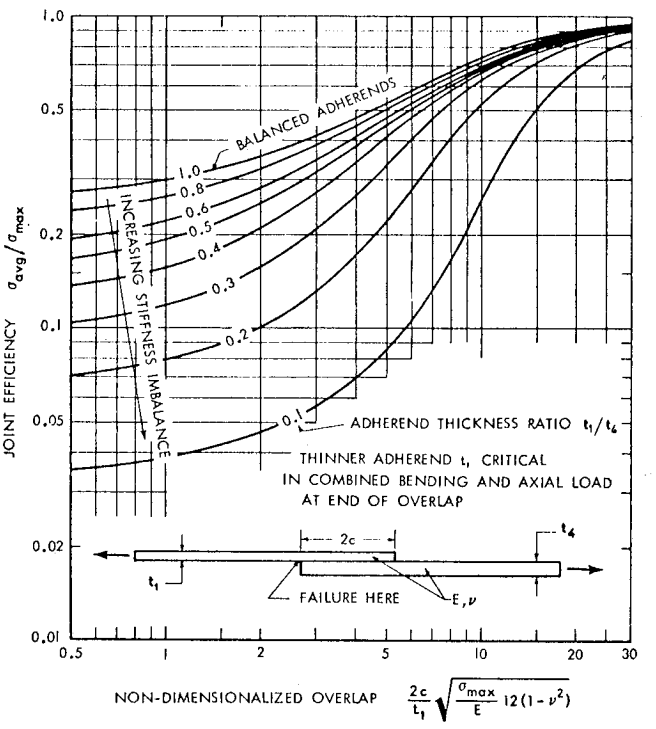

FIGURE 28. EFFECT OF ADHEREND STIFFNESS IMBALANCE ON STRENGTH OF SINGLE-LAP BONDED JOINTS

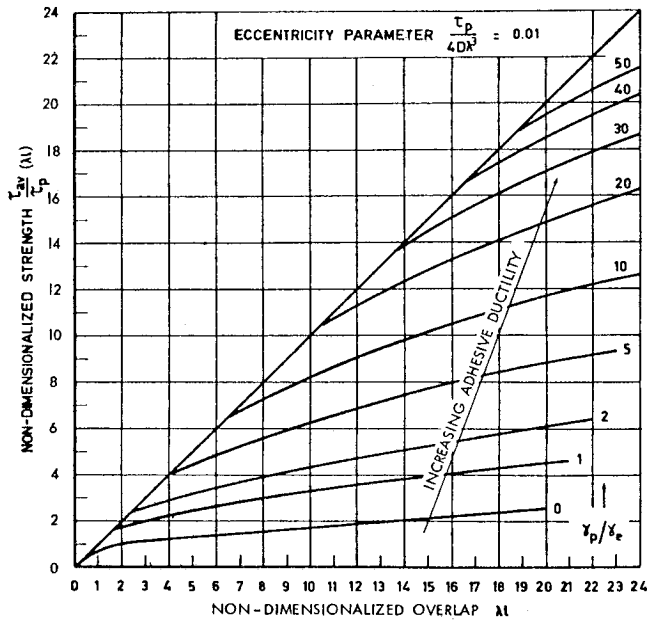

FIGURE 29. SHEAR STRENGTHS OF BALANCED SINGLE-LAP BONDED JOINTS

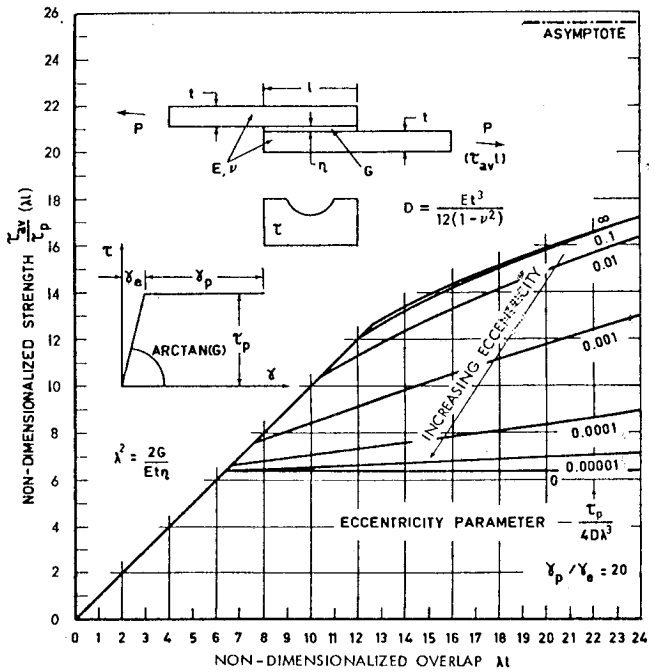

FIGURE 30. INFLUENCE OF ECCENTRICITY ON BOND SHEAR STRENGTH OF SINGLE-LAP BONDED JOINTS

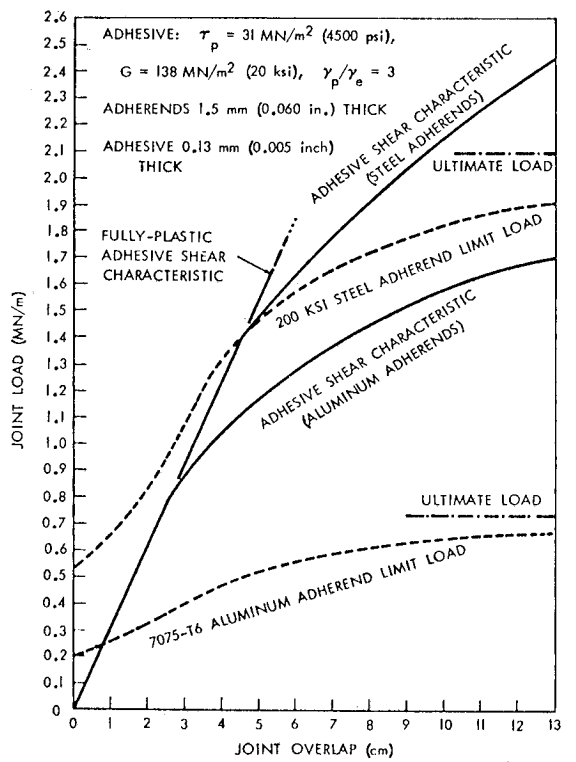

FIGURE 31. INFLUENCE OF ADHEREND MATERIAL ON STRENGTH OF SINGLE-LAP BONDED JOINTS

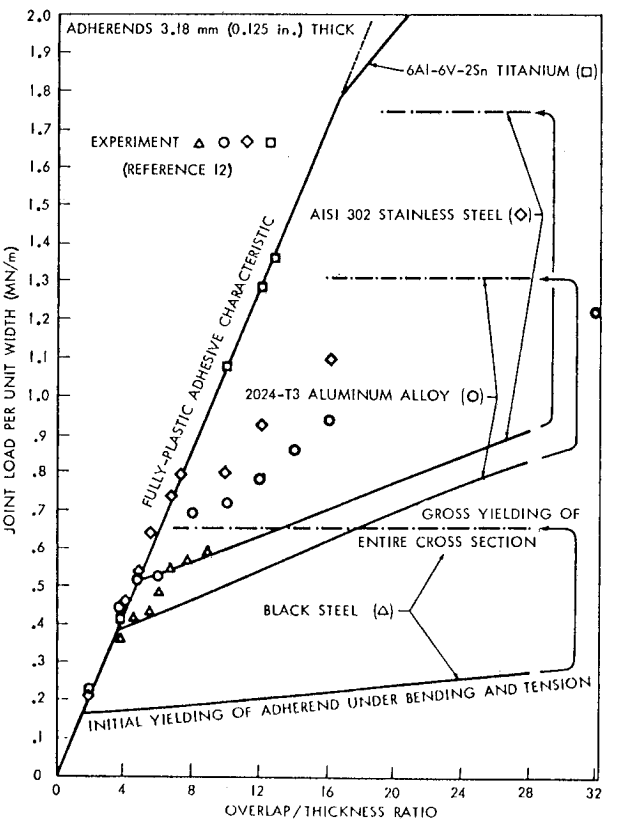

FIGURE 32. COMPARISON BETWEEN THEORY AND EXPERIMENT FOR SINGLE-LAP JOINTS (VARIOUS METAL ADHERENDS OF THE SAME THICKNESS)

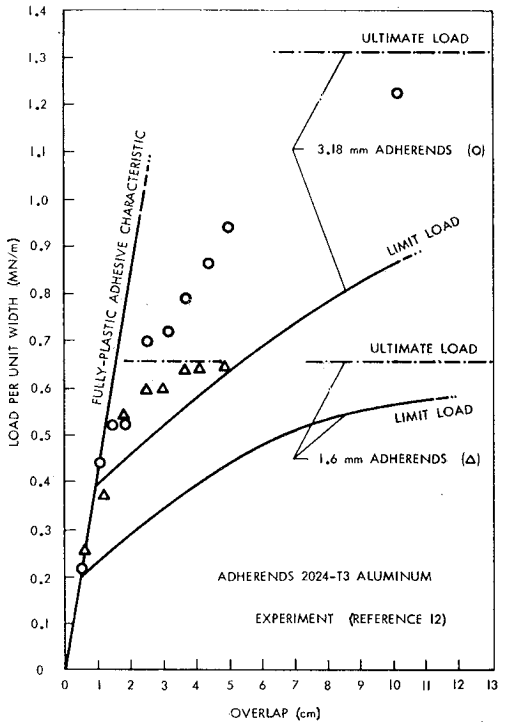

FIGURE 33. COMPARISON BETWEEN THEORY AND EXPERIMENT FOR SINGLE-LAP JOINTS (ALUMINUM ADHERENDS OF DIFFERENT THICKNESSES

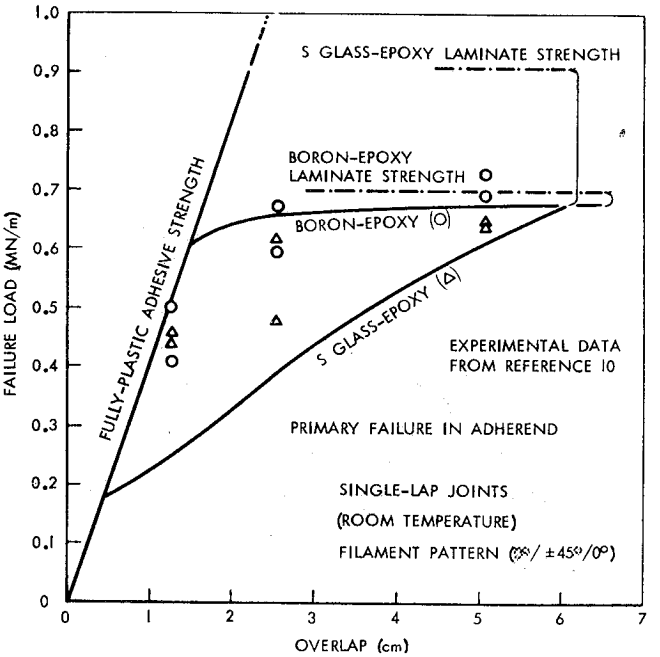

FIGURE 34. COMPARISON BETWEEN THEORY AND EXPERIMENT FOR SINGLE-LAP BONDED JOINTS USING COMPOSITE ADHERENDS

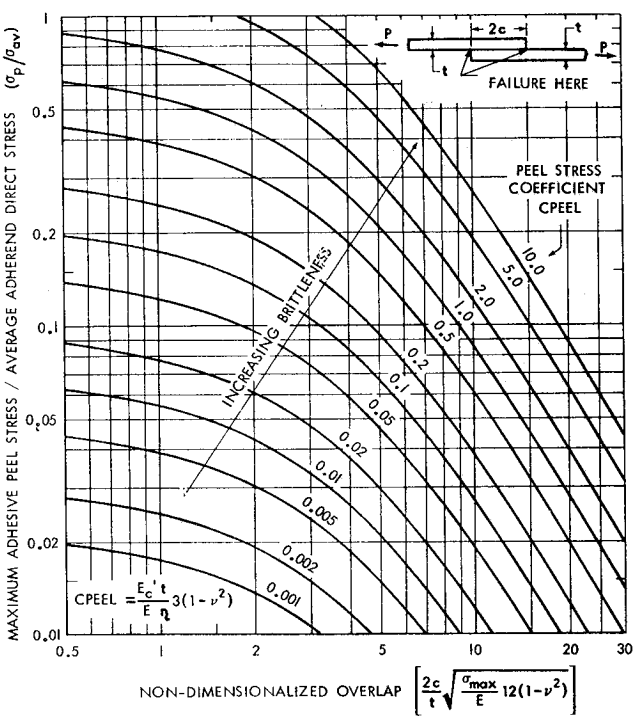

FIGURE 35. PEEL STRESSES IN BALANCED SINGLE-LAP JOINTS

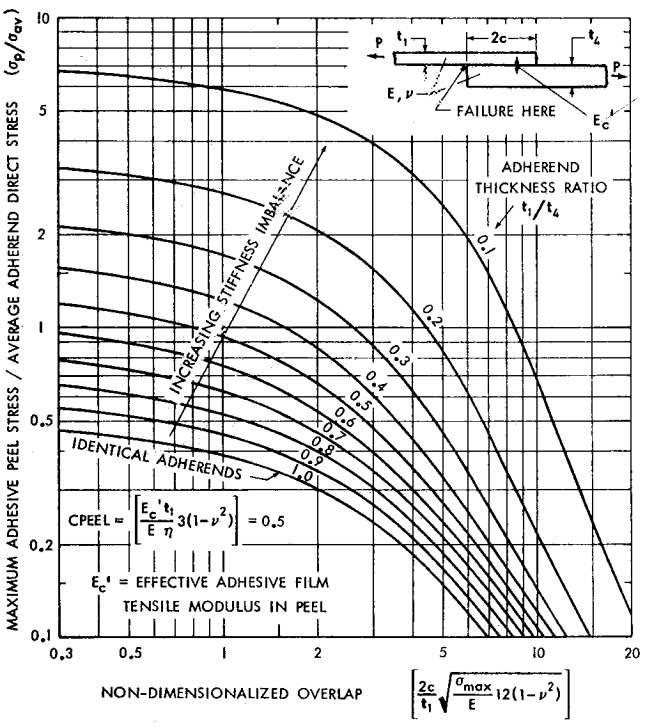

FIGURE 36. EFFECT OF ADHEREND STIFFNESS IMBALANCE ON PEEL STRESSES IN SINGLE-LAP JOINTS

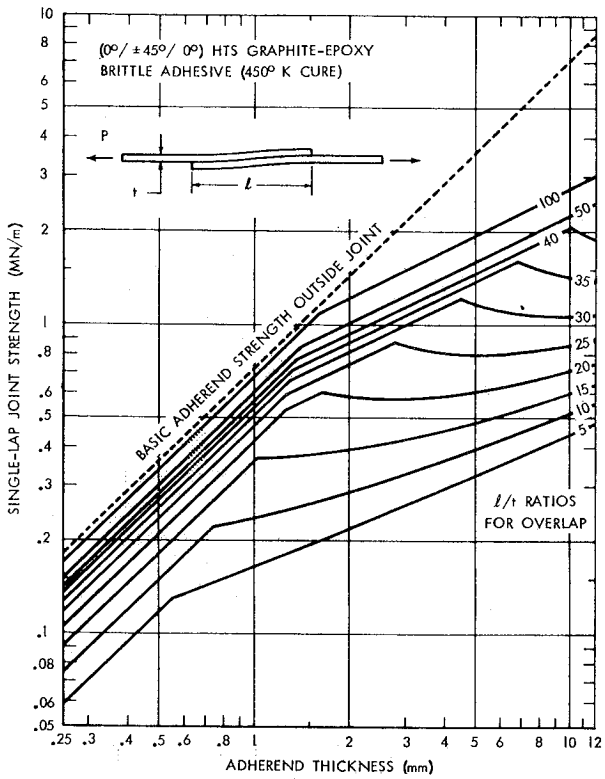

FIGURE 37. STRENGTH OF SINGLE-LAP BONDED COMPOSITE JOINTS

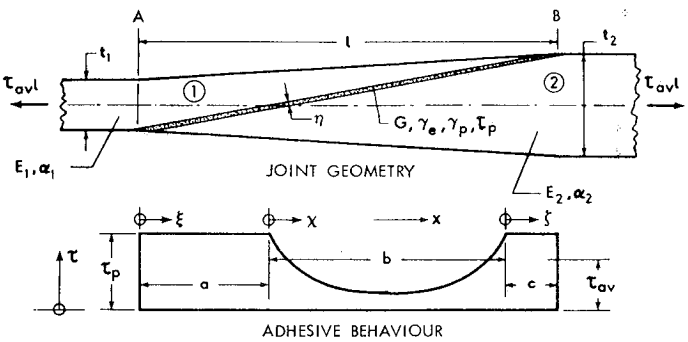

FIGURE 38. JOINT GEOMETRY AND ADHESIVE BEHAVIOR FOR BONDED SCARF JOINT

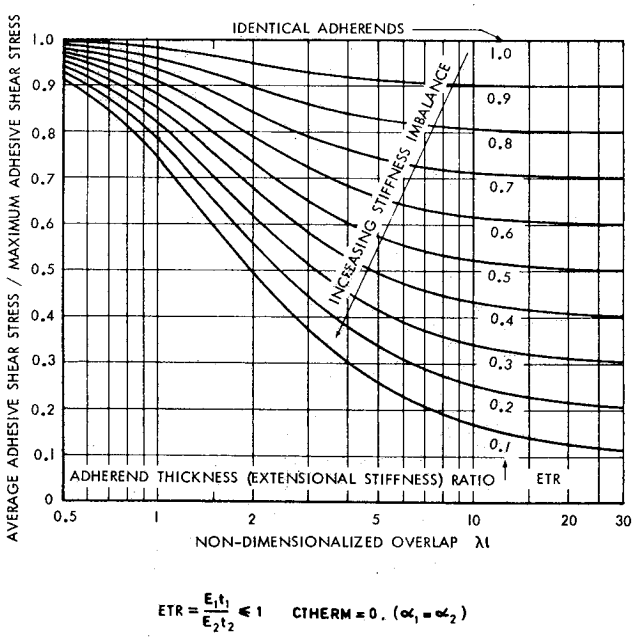

$$ETR = \frac{E_1 t_1}{E_2 t_2} \leq 1 \qquad CTHERM = 0,\ (\alpha_1 = \alpha_2)$$

LOCATION A IS CRITICAL FOR BOTH POSITIVE (TENSILE LAP-SHEAR) AND NEGATIVE (COMPRESSIVE LAP-SHEAR) VALUES OF LOAD P

FIGURE 39. EFFECT OF ADHEREND STIFFNESS IMBALANCE ON ELASTIC STRENGTH OF BONDED SCARF JOINTS

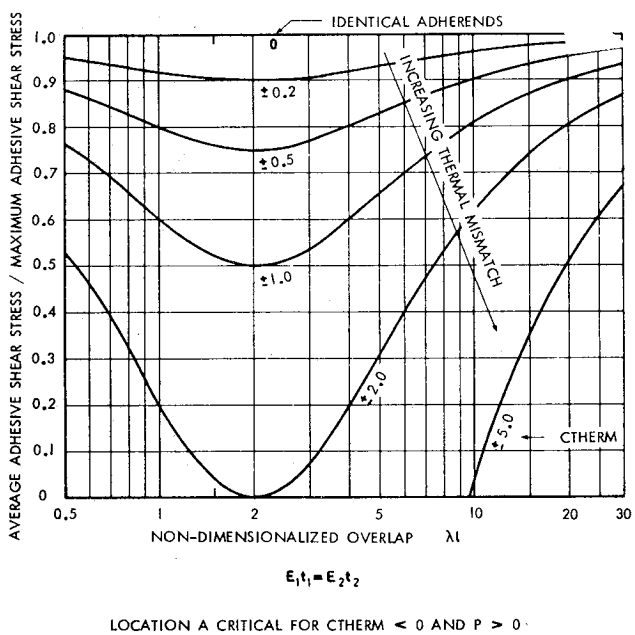

$$E_1 t_1 = E_2 t_2$$

LOCATION A CRITICAL FOR CTHERM < 0 AND P > 0
LOCATION A CRITICAL FOR CTHERM > 0 AND P < 0
LOCATION B CRITICAL FOR CTHERM < 0 AND P < 0
LOCATION B CRITICAL FOR CTHERM > 0 AND P > 0

FIGURE 40. EFFECT OF ADHEREND THERMAL MISMATCH ON ELASTIC STRENGTH OF BONDED SCARF JOINTS

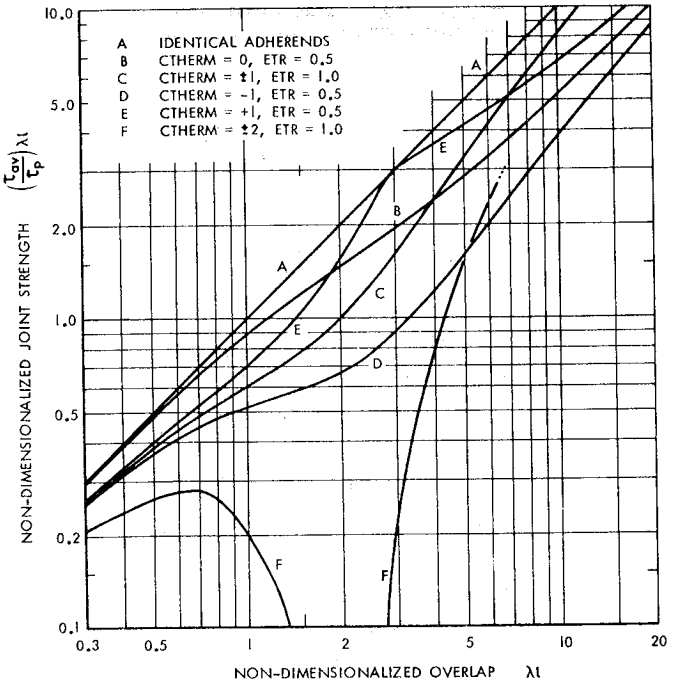

FIGURE 41. INTERACTION OF ADHEREND STIFFNESS AND THERMAL IMBALANCES FOR ELASTIC BONDED SCARF JOINTS

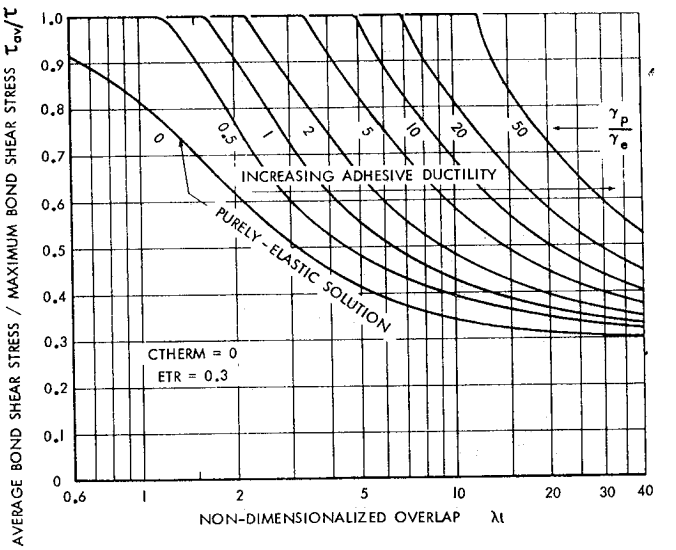

FIGURE 42. EFFECT OF ADHESIVE PLASTICITY ON BOND STRENGTH FOR STIFFNESS-IMBALANCED SCARF JOINTS

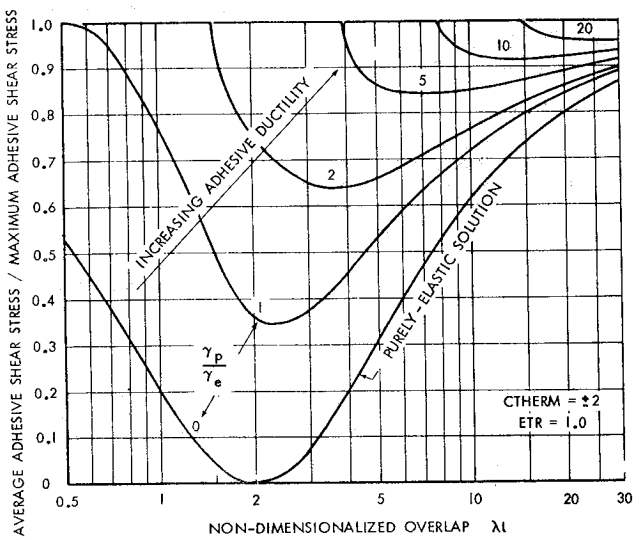

FIGURE 43. EFFECT OF ADHESIVE PLASTICITY ON BOND STRENGTH FOR THERMALLY-MISMATCHED SCARF JOINTS

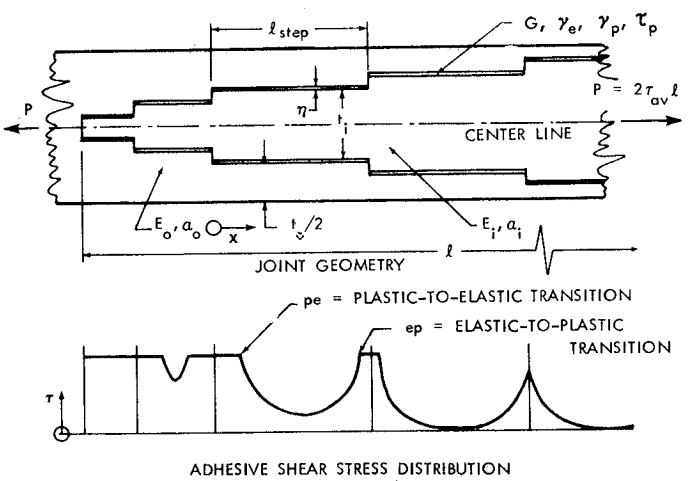

FIGURE 44. JOINT GEOMETRY AND ADHESIVE BEHAVIOR FOR BONDED STEPPED-LAP JOINTS

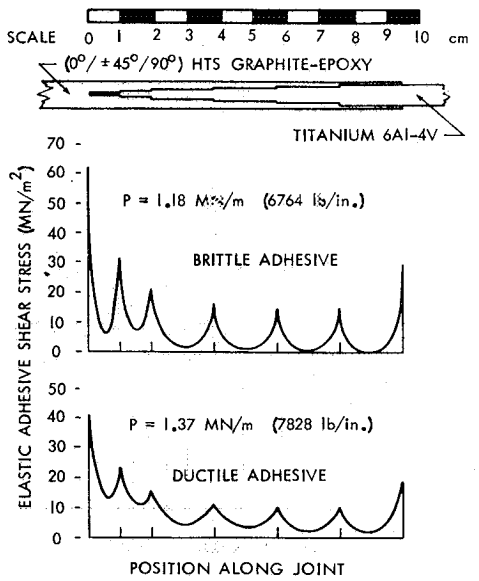

FIGURE 45. ELASTIC SHEAR STRESS DISTRIBUTIONS FOR BRITTLE AND DUCTILE ADHESIVES IN BONDED STEPPED-LAP JOINTS

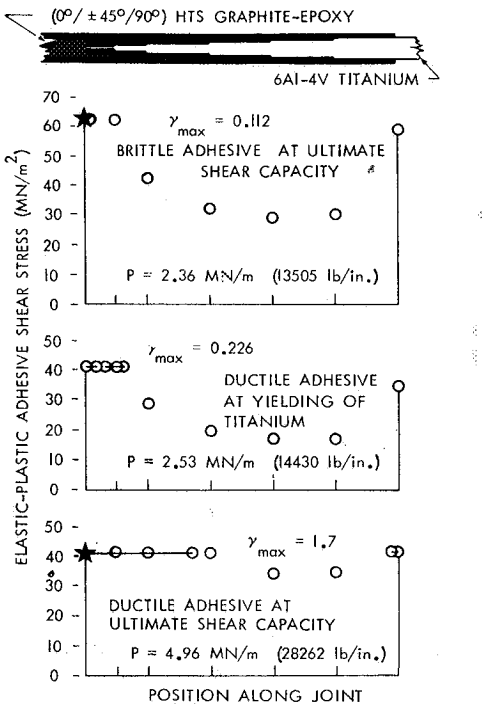

FIGURE 46. ELASTIC-PLASTIC SHEAR STRESS DISTRIBUTIONS FOR BRITTLE AND DUCTILE ADHESIVES IN BONDED STEPPED-LAP JOINTS

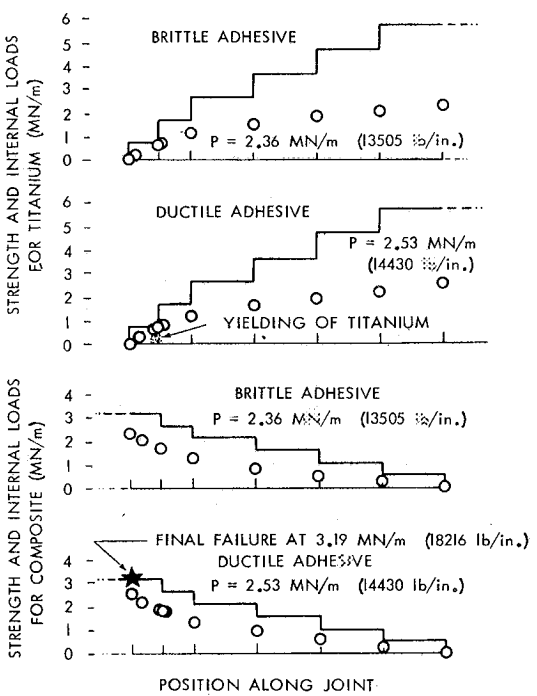

FIGURE 47. ADHEREND STRENGTHS AND INTERNAL LOADS FOR BONDED STEPPED-LAP JOINTS

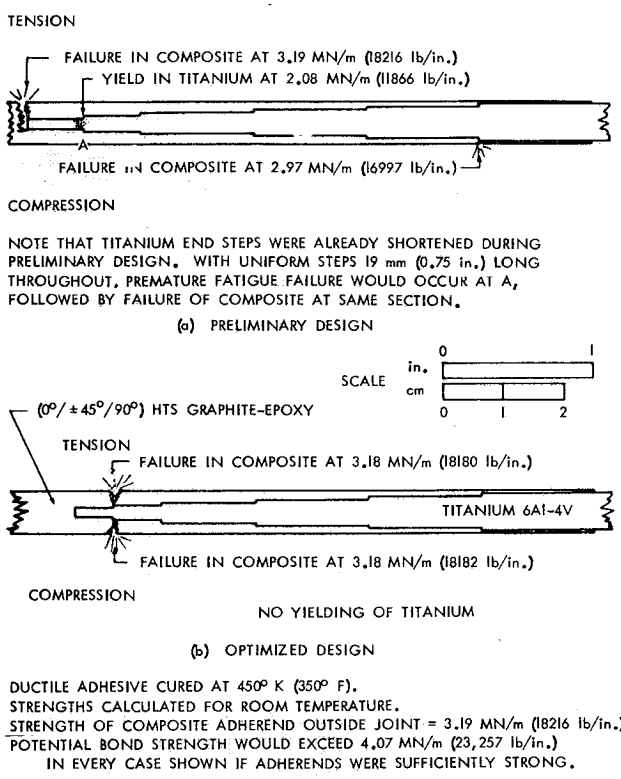

FIGURE 48. OPTIMIZATION OF DETAILS IN STEPPED-LAP BONDED JOINTS

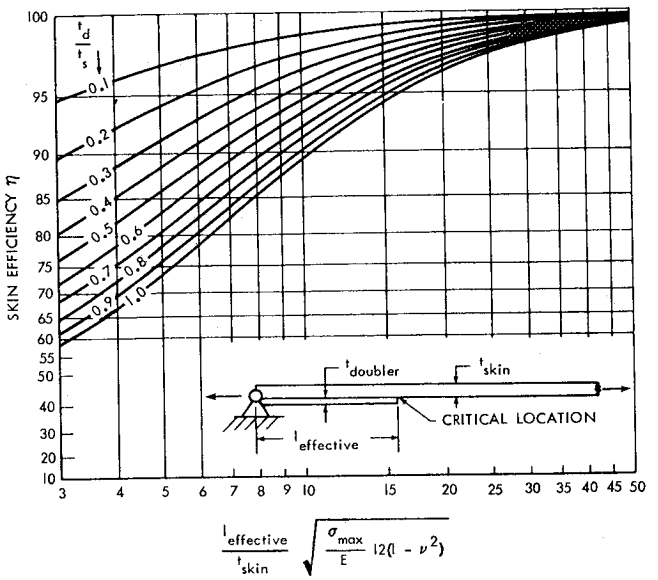

FIGURE 49. SKIN EFFICIENCY FOR BONDED DOUBLERS (SIMPLY-SUPPORTED EDGE CONDITIONS)

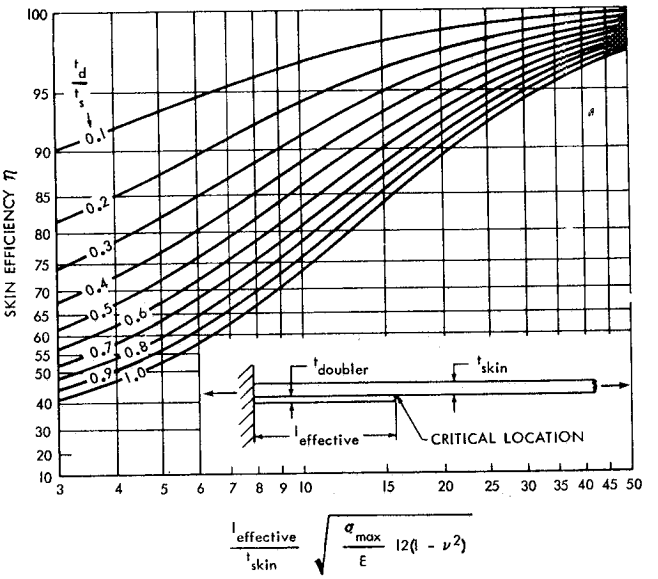

FIGURE 50. SKIN EFFICIENCY FOR BONDED DOUBLERS (BUILT-IN EDGE CONDITIONS)

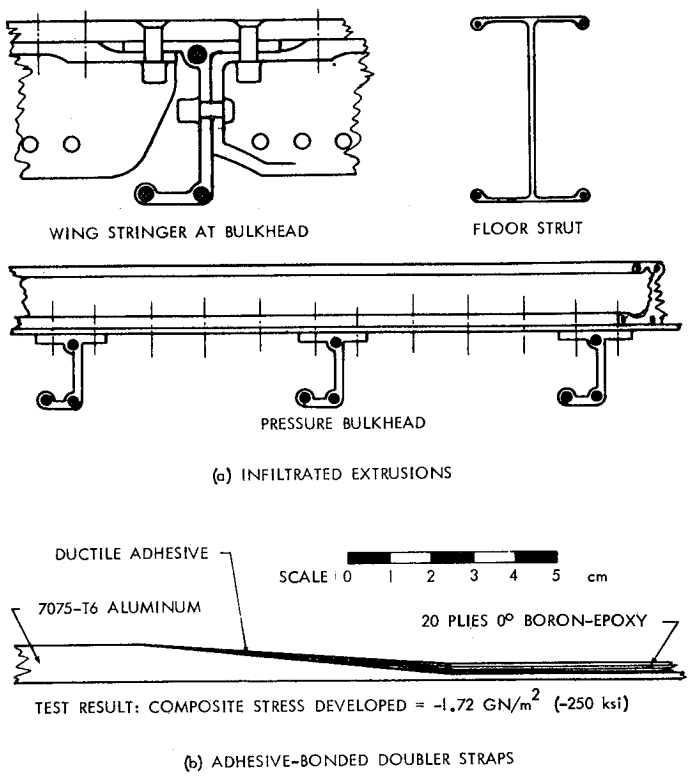

FIGURE 51. SELECTIVE REINFORCEMENT OF METAL STRUCTURE BY BONDED ADVANCED COMPOSITES

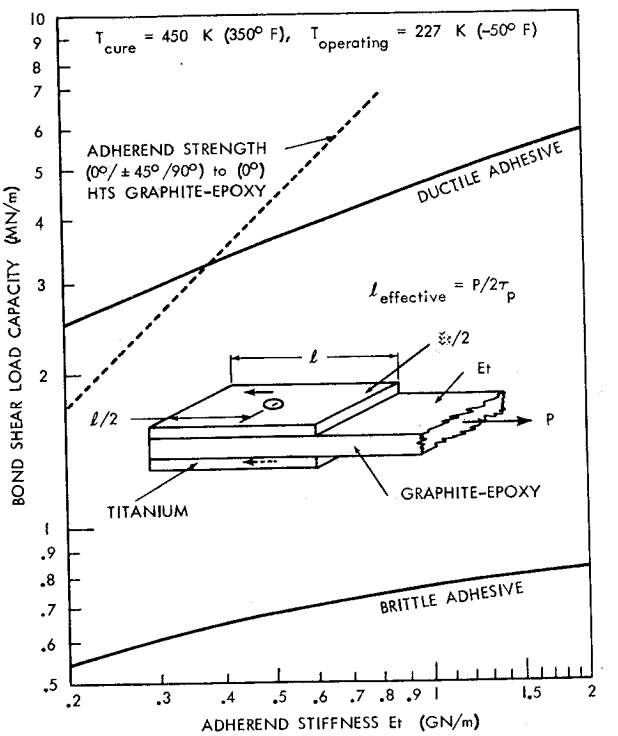

FIGURE 52. BONDED METAL DOUBLERS AROUND BOLT HOLE IN COMPOSITES

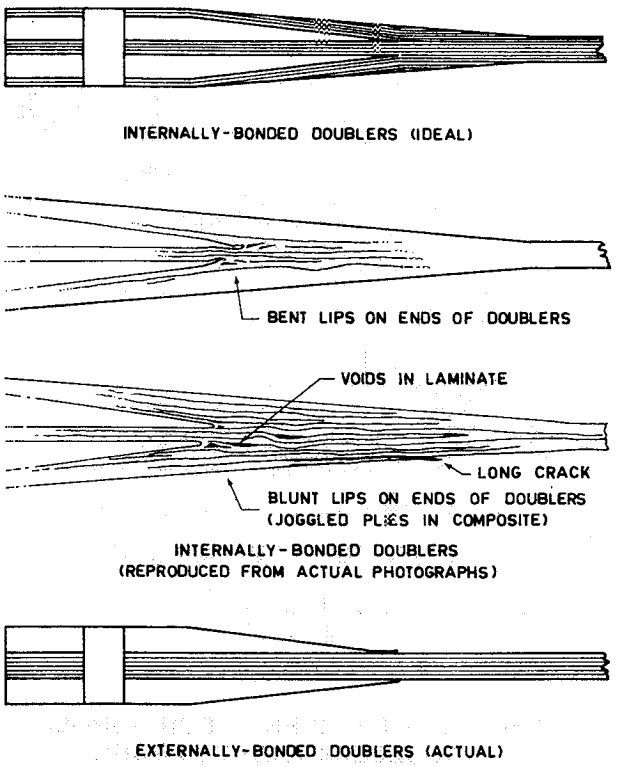

FIGURE 53. INTERNAL AND EXTERNAL BONDED METAL DOUBLERS

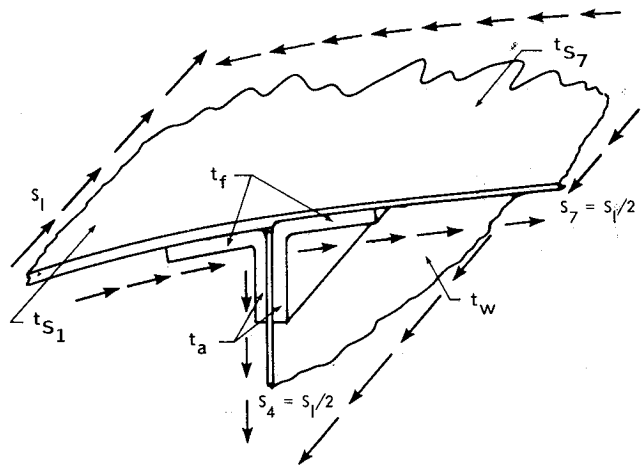

FIGURE 54. BONDED JOINT CONFIGURATION FOR MULTI-CELL TORSION BOX

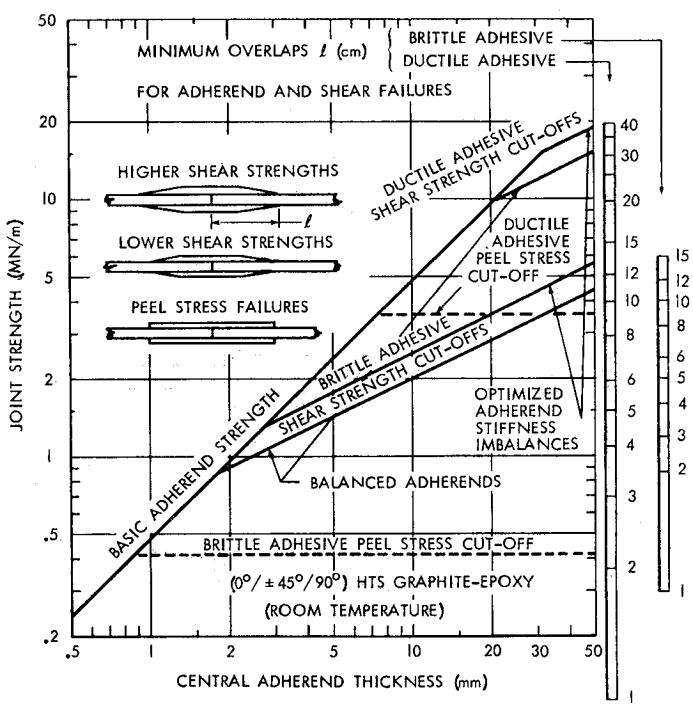

FIGURE 55. PEEL STRESS ALLEVIATION OF DOUBLE-LAP BONDED JOINTS

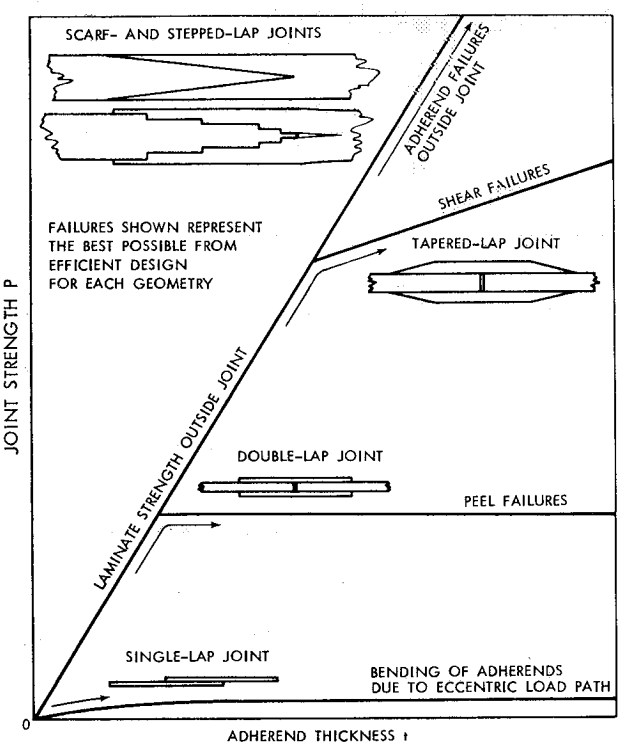

FIGURE 56. INFLUENCE OF JOINT SIZE ON SELECTION OF JOINT CONFIGURATION

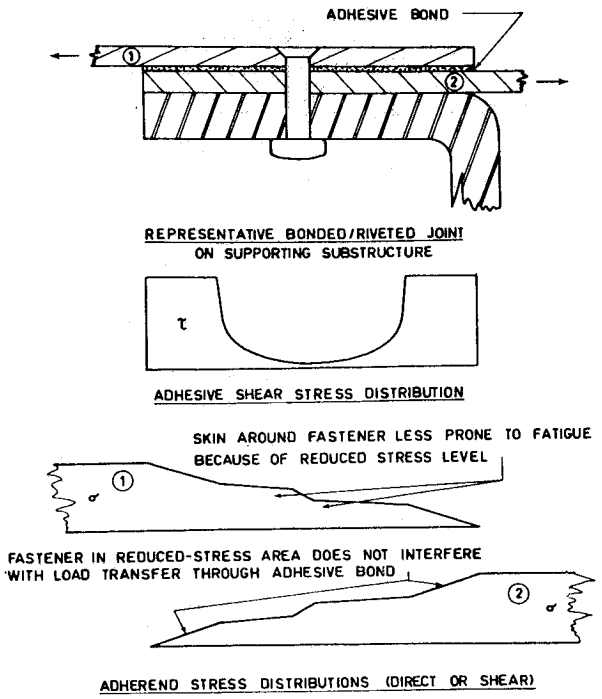

FIGURE 57. MOMENT RESTRAINT IN SINGLE-LAP JOINT AND LOAD TRANSFER IN BONDED/BOLTED JOINT

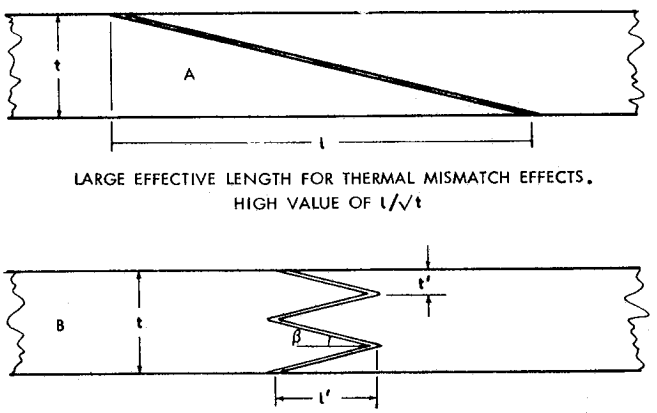

FIGURE 59. THERMAL STRESS ALLEVIATION TECHNIQUE FOR BONDED SCARF JOINTS

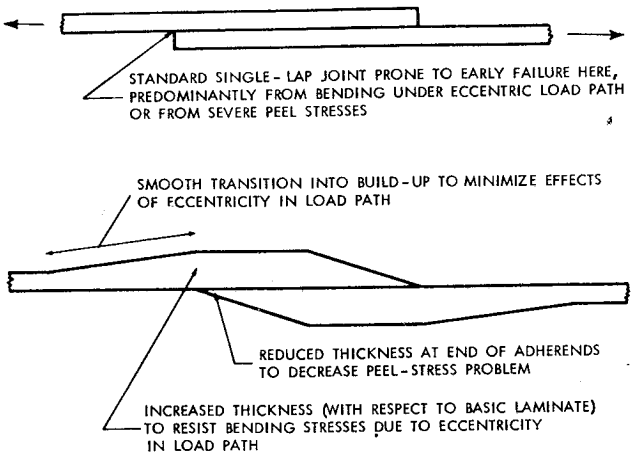

FIGURE 58. IMPROVED EFFICIENCY OF UNSUPPORTED SINGLE-LAP JOINTS

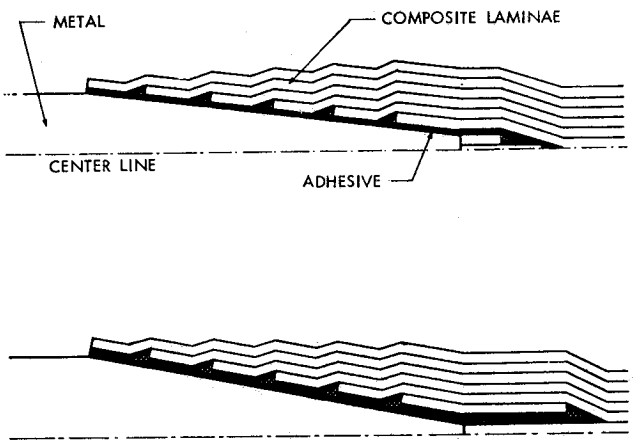

FIGURE 60. STRESS CONCENTRATION RELIEF AT TIP OF STEPPED-LAP JOINTS

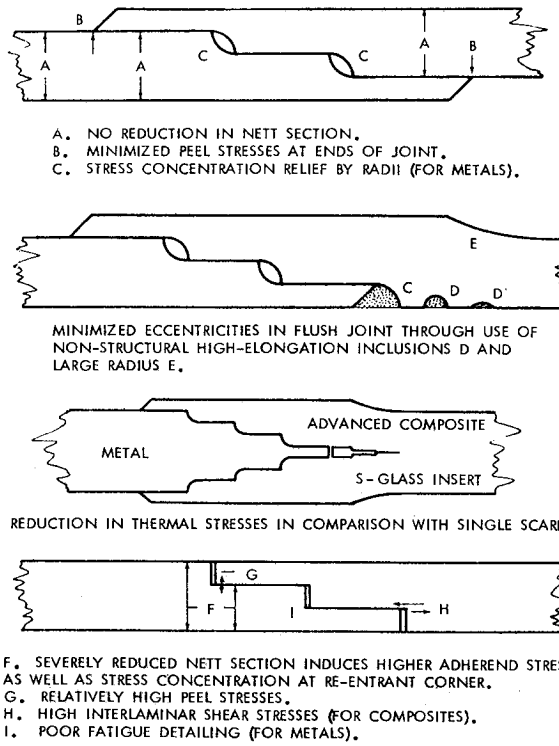

FIGURE 61. GOOD AND POOR DESIGN PRACTICE FOR STEPPED-LAP BONDED JOINTS

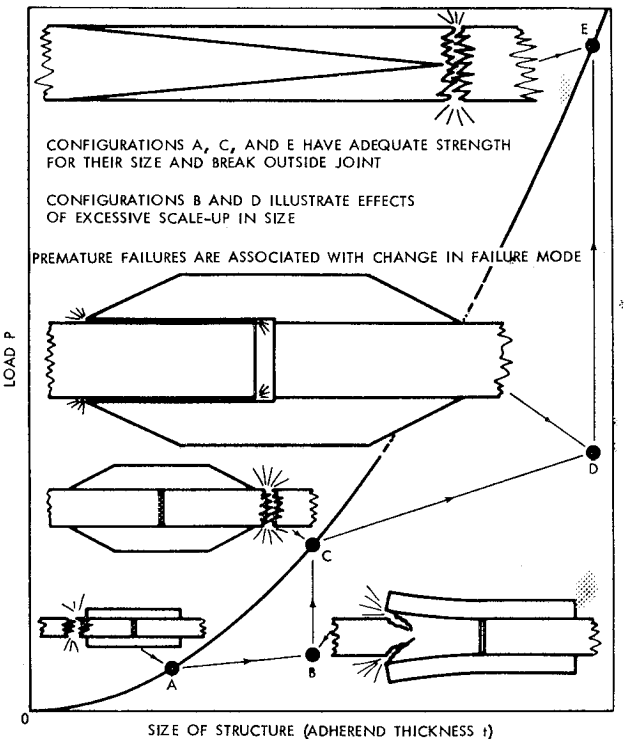

FIGURE 62. PROBLEMS WITH SCALE-UP OF BONDED JOINT STRENGTHS

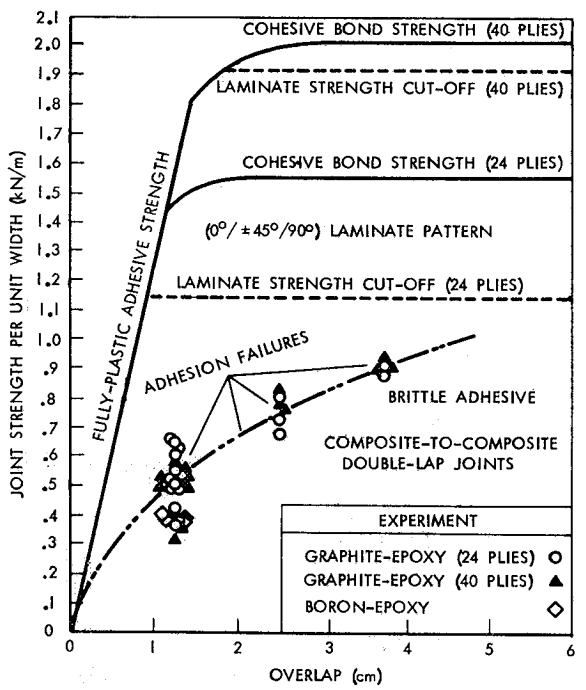

FIGURE 63. COMPARISON OF THEORY AND EXPERIMENT SHOWING LOSS OF STRENGTH ATTRIBUTABLE TO ADHESION FAILURES

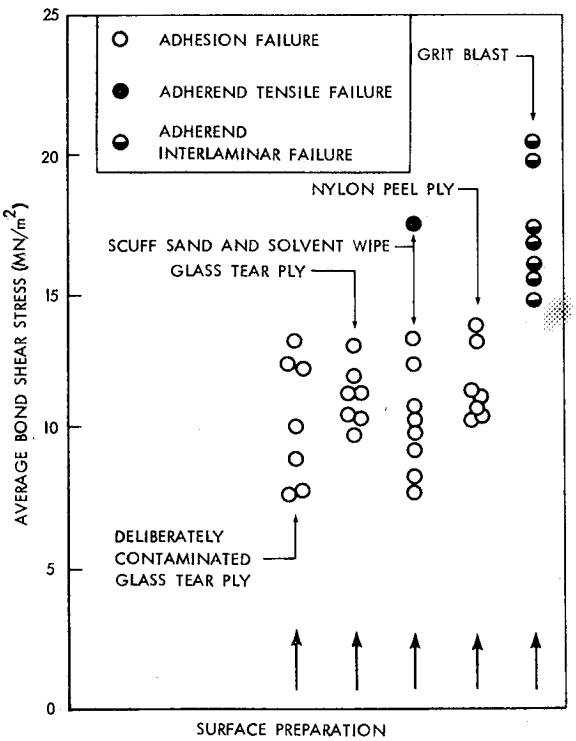

FIGURE 64. EFFECT OF SURFACE PREPARATION ON STRENGTH OF BONDED JOINTS